JOURNAL OF PETROLOGY

Journal of Petrology, 2021, 1–25
doi: 10.1093/petrology/egab025
Advance Access Publication Date: 20 March 2021
Original Manuscript

OXFORD

Evolution of Intraplate Alkaline to Tholeiitic Basalts via Interaction Between Carbonated Melt and Lithospheric Mantle

Ze-Zhou Wang[1,2] and Sheng-Ao Liu [1]*

[1]State Key Laboratory of Geological Processes and Mineral Resources, China University of Geosciences, Beijing 100083, China; [2]Isotope Laboratory, Department of Earth and Space Sciences, University of Washington, Seattle, WA 98195, USA

*Corresponding author. E-mail: lsa@cugb.edu.cn Tel: +86-10-82322382; fax:+86-10-82322382

Received 12 October 2020; Accepted 12 March 2021

ABSTRACT

Intraplate basaltic volcanism commonly exhibits wide compositional ranges from silica-undersaturated alkaline basalts to silica-saturated tholeiitic basalts. Possible mechanisms for the compositional transition involve variable degrees of partial melting of a same source, decompression melting at different mantle depths (so-called 'lid effect'), and melt-peridotite interaction. To discriminate between these mechanisms, here we investigated major-trace elemental and Sr–Nd–Mg–Zn isotopic compositions of a suite of intraplate alkaline and tholeiitic basalts from the Datong volcanic field in eastern China. Specifically, we employed Mg and Zn isotope systematics to assess whether the silica-undersaturated melts originated from a carbonated mantle source. The alkaline basalts have young HIMU-like Sr and Nd isotopic compositions, lower δ^{26}Mg (-0·42‰ to -0·38‰) and higher δ^{66}Zn (0·40‰ to 0·46‰) values relative to the mantle. These characteristics were attributable to an asthenospheric mantle source hybridized by carbonated melts derived from the stagnant Pacific slab in the mantle transition zone. From alkaline to tholeiitic basalts, δ^{26}Mg gradually increases from -0·42‰ to -0·28‰ and δ^{66}Zn decreases from 0·46‰ to 0·28‰ with decreasing alkalinity and incompatible trace element abundances (e.g. Rb, Nb, Th and Zr). The Mg and Zn isotopic variations are significantly beyond the magnitude (<0·1‰) induced by different degrees of fractional crystallization and partial melting of a same mantle source, excluding magmatic differentiation, different degrees of partial melting and the 'lid effect' as possible mechanisms accounting for the compositional variations in the Datong basalts. There are strong, near-linear correlations of δ^{26}Mg and δ^{66}Zn with $^{87}Sr/^{86}Sr$ (R^2=0·75 – 0·81) and $^{143}Nd/^{144}Nd$ (R^2=0·83 – 0·90), suggesting an additional source for the Datong basalts. This source is characterized by pristine mantle-like δ^{26}Mg and δ^{66}Zn values as well as EM1-like Sr–Nd isotopic ratios, pointing towards a metasomatized subcontinental lithospheric mantle (SCLM). Isotope mixing models show that mingling between alkaline basaltic melts and partial melts from the SCLM imparts all the above correlations, which means that the SCLM must have been partially melted during melt-SCLM reaction. Our results underline that interaction between carbonated silica-undersaturated basaltic melts and the SCLM acts as one of major processes leading to the compositional diversity in intracontinental basaltic volcanism.

Key words: alkaline basalts; tholeiitic basalts; carbonated melt-lithosphere interaction; Mg isotopes; Zn isotopes

INTRODUCTION

Basaltic volcanism erupted in intraplate settings (e.g. oceanic hotspot, intracontinental volcano and continental rift) provides solid evidence for recycling of crustal materials into the deep mantle owing to their variable and enriched radiogenic isotopic signatures

(Hofmann, 2014). Regardless, intraplate basaltic volcanism commonly spans a wide and continuous composition ranging from nepheline-normative alkaline basalts to hypersthene/quartz-normative tholeiitic basalts, but the origin is still debated. The alkaline to tholeiitic transition is generally accompanied by a decrease in incompatible element concentrations with increasing silica saturation, which has been often ascribed to increasing degrees of mantle partial melting (e.g. Chen *et al.*, 1991; Wilson *et al.*, 1995; Lustrino *et al.*, 2002; Melluso et al., 2016). However, experimental studies demonstrate that varying extents of partial melting of potential source lithologies (peridotite, pyroxenite or hornblendite) with or without CO_2 alone fails to reproduce the full compositional spectrum observed in natural basalts (Hirose, 1997; Walter, 1998; Hirschmann *et al.*, 2003; Kogiso *et al.*, 2003; Wasylenki *et al.*, 2003; Keshav *et al.*, 2004; Kogiso & Hirschmann, 2006; Dasgupta *et al.*, 2007; Pilet *et al.*, 2008; Gerbode & Dasgupta, 2010; Dasgupta *et al.*, 2013). Alternatively, this transition may be caused by interaction between silicate melt and peridotite as suggested by the 'sandwich' experiments, during which the silica-undersaturation of reacted melts could change drastically because of dissolution of olivine or pyroxene in melts (Pilet *et al.*, 2008; Lambart *et al.*, 2012; Mallik & Dasgupta, 2014). This hypothesis can be tested in natural samples by combining major and trace elements with isotopes. For instance, coherent variations in major-trace elements and radiogenic isotopes have been regarded as evidence for melt-lithospheric mantle interaction in producing different types of intraplate lavas (Lassiter & DePaolo, 1997; Zhang *et al.*, 2017). Nonetheless, radiogenic isotopes are commonly insufficient to exclusively fingerprint recycled carbonates in the mantle, which have been advocated to play a fundamental role in the generation of silica-undersaturated alkaline basalts (Hirose, 1997; Dasgupta *et al.*, 2007).

Like radiogenic Sr, Nd and Pb isotopes, the fractionation of stable Mg and Zn isotopes during mantle melting and basaltic differentiation is negligible or limited ($\leq$0·1‰) due to minimal melt-mineral isotope fractionation at magmatic temperatures (Chen *et al.*, 2013; Teng, 2017; Wang *et al.*, 2017*b*; Zhong *et al.*, 2017; Sossi *et al.*, 2018; Stracke *et al.*, 2018). On the other hand, Mg and Zn isotopes have an ability of tracking recycled carbonates in basalt sources (Liu & Li, 2019 and references therein). Sedimentary carbonates are characterized by extremely lower δ^{26}Mg and higher δ^{66}Zn compared with the mantle and subducted silicate components such as serpentinite, altered oceanic crust and silicate-dominated sediments (Fig. 1). Hence, basaltic melts derived from a mantle source hybridized by recycled carbonate or carbonated oceanic crust are expected to have distinctively lighter Mg and heavier Zn isotopic compositions than melts derived from uncontaminated mantle, which have been observed in many intraplate silica-undersaturated alkaline basalts (e.g. Liu & Li, 2019; Beunon *et al.*, 2020; Liu *et al.*, 2020; Li *et al.*, 2021). Systematic Mg and Zn isotopic variations across alkaline and tholeiitic basalts should also be envisaged if the alkaline to tholeiitic transition results from interaction of carbonated silica-undersaturated melt with peridotite (e.g. Zhang *et al.*, 2017). That is, if the isotopic variations significantly exceed the magnitude of isotopic fractionation induced by partial melting and magmatic differentiation, a role of carbonated melt–peridotite reaction may be recognized. Therefore, Mg and Zn isotopic systematics offer novel approaches to discriminating the proposed mechanisms of producing the wide compositional spectrum of intraplate basalts.

Intraplate basaltic volcanism has occurred widely in eastern China along the eastern margin of Euro-Asian continent since the Late Mesozoic. These basalts range from nephelinite, basanite, alkali olivine basalt to tholeiite and display a wide range in elemental and radiogenic isotopic compositions comparable to that of global intraplate basalts (e.g. Zhou & Armstrong, 1982; Basu *et al.*, 1991; Fan & Hooper, 1991; Zou *et al.*, 2000; Xu *et al.*, 2005; Liu *et al.*, 2008; Zeng *et al.*, 2010, 2011; Sakuyama *et al.*, 2013), thus providing ideal samples for deciphering the origin of the compositional continuum in intraplate volcanism. To date, the cause of compositional evolution of intraplate basalts from eastern China remains controversial. For example, a recent study proposed that the lithospheric thickness exerts the primary control on the compositions of these basalts in terms of the extent and pressure of mantle melting (so-called 'lid effect'; Guo *et al.*, 2020), whereas earlier studies suggested that interaction of asthenosphere-derived magma with lithospheric mantle results in the transition from alkaline to tholeiitic basalts (Xu *et al.*, 2005; Tang *et al.*, 2006; Wang *et al.*, 2018*b*). In this study, we carried out combined analyses of petrology, major and trace elements and Sr–Nd–Mg–Zn isotopes on Quaternary alkaline and tholeiitic basalts from the Datong volcanic field, which is a famous intraplate monogenetic volcanic region in eastern China and has been extensively studied in various disciplines, including petrology, geochronology, geochemistry, geophysics and paleomagnetism (e.g. Xu *et al.*, 2005; Yamamoto *et al.*, 2007; Zhao *et al.*, 2015; Zhang *et al.*, 2016; Sun *et al.*, 2019). Our results provide strong evidence for reaction of carbonated silicate melts with the lithospheric mantle as one of the main mechanisms responsible for the alkaline to tholeiitic transition commonly observed in intracontinental basaltic magmatism.

REGIONAL GEOLOGY AND SAMPLE DESCRIPTION

Cenozoic basalts in eastern China are widely distributed in four tectonic regions: NE China, North China Craton, South China Block and Hainan Island (Fig. 2), extending over 4000 km from north to south. The lithology is dominated by alkaline basalts, with minor tholeiitic basalts (Zhou & Armstrong, 1982). Their eruption age is mostly Neogene to Pleistocene (Li *et al.*, 2017). The spatial distribution of these lavas is in accordance with a

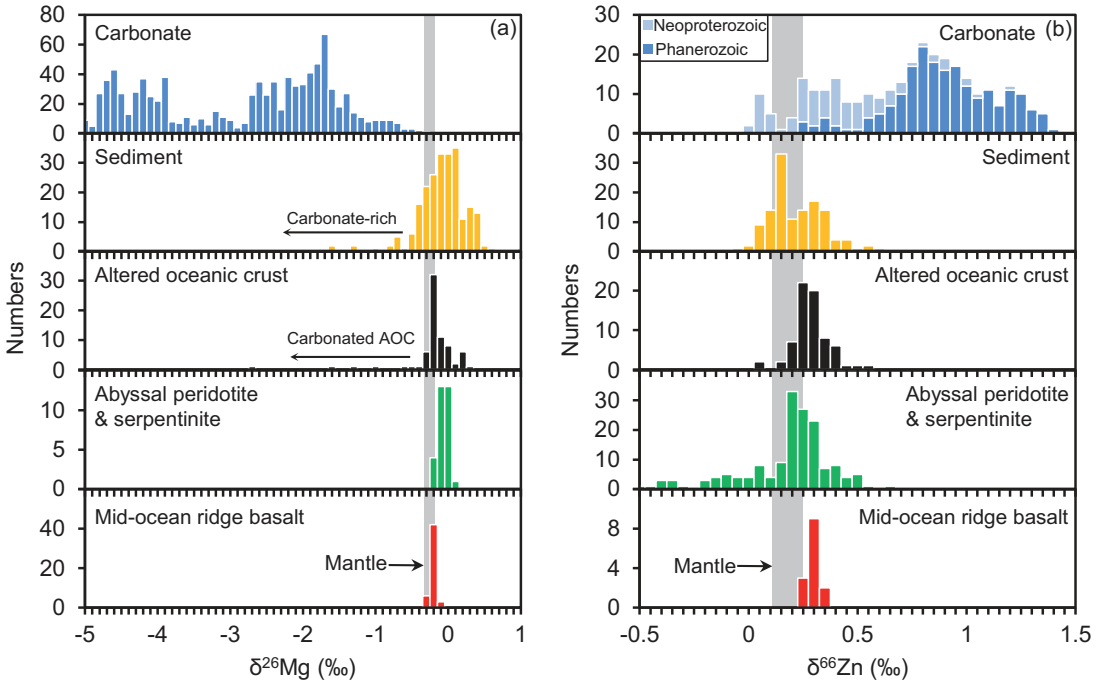

Fig. 1. Summary of (a) Mg and (b) Zn isotopic compositions of the main components in subducting slabs. Data sources: Carbonates: δ^{26}Mg,Teng (2017) and references therein; δ^{66}Zn, Pichat *et al.* (2003), Kunzmann *et al.* (2013), Liu *et al.* (2017*b*), Sweere *et al.* (2018), Wang *et al.* (2018*a*) and Lv *et al.* (2018); low δ^{66}Zn values of some Neoproterozoic carbonates were interpreted to be the consequence of post-depositional diagenesis (Lv *et al.*, 2018). Sediments: δ^{26}Mg, Li *et al.* (2010, 2014*b*), Huang *et al.* (2013), Wimpenny *et al.* (2014), Ma *et al.* (2015), Wang *et al.* (2015), Teng *et al.* (2016) and Hu *et al.* (2017); δ^{66}Zn, Bentahila *et al.* (2008), Pons *et al.* (2011), Little *et al.* (2016) and Inglis *et al.* (2017). Altered oceanic crust (AOC): δ^{26}Mg, Huang *et al.* (2015*a*, 2018*c*); δ^{66}Zn, Huang *et al.* (2016) and Inglis *et al.* (2017). Abyssal peridotites and serpentinites: δ^{26}Mg, Liu *et al.*, 2017*a*; δ^{66}Zn, Pons *et al.* (2011, 2016), Debret *et al.* (2018*a*, 2018*b*) and Liu *et al.* (2019). Mid-ocean ridge basalt: δ^{26}Mg, Teng *et al.* (2010); δ^{66}Zn, Wang *et al.* (2017*b*) and Huang *et al.* (2018*b*). The grey vertical bar represents the average mantle value estimated from mantle peridotites (δ^{26}Mg = -0·25 ± 0·04‰, Teng *et al.*, 2010; δ^{66}Zn = 0·17 ± 0·08‰, Doucet *et al.*, 2016; Wang *et al.*, 2017*b*; Huang *et al.*, 2018*a*; Sossi *et al.*, 2018; Huang *et al.*, 2019; Liu *et al.*, 2019).

large scale low-velocity zone (~100–400 km depth) above the mantle transition zone (MTZ), where the subducted western Pacific slab stagnates at present as revealed by seismic tomography (Fig. 2a; Huang & Zhao, 2006; Fukao *et al.*, 2009; Liu *et al.*, 2017*c*). Thus, Cenozoic intraplate basaltic volcanism in eastern China has been commonly reckoned to be genetically related to the stagnant Pacific slab (e.g. Zhao *et al.*, 2009; Sakuyama *et al.*, 2013; Liu *et al.*, 2016; Li *et al.*, 2017 ; Li and Wang, 2018; Xu *et al.*, 2018, 2020). Their mantle sources could have been metasomatized by crustal components derived from the stagnant slab, as indicated by OIB-like chemical and radiogenic isotopic compositions of these basalts (e.g. Zhou & Armstrong, 1982; Zhi *et al.*, 1990; Basu *et al.*, 1991; Zou *et al.*, 2000; Tang *et al.*, 2006; Zeng *et al.*, 2011; Sakuyama *et al.*, 2013; Xu *et al.*, 2018). In particular, recent Mg–Fe–Zn isotopic studies on these basalts suggest that deeply subducted carbonates may play an important role in oxidizing the mantle and facilitating the formation of silica-understatured alkaline lavas (Yang *et al.*, 2012; Huang *et al.*, 2015*b*; Liu *et al.*, 2016; Tian *et al.*, 2016; Li *et al.*, 2017; Wang *et al.*, 2017*a*, 2018*b*; He *et al.*, 2019; Jin *et al.*, 2020; Cai *et al.*, 2021).

Cenozoic basaltic volcanism in the North China Craton occurs predominantly adjacent to the rifts or fault zones within the Trans-North China Orogen and the Tan-Lu Fault of the Eastern Block (Fig. 2b). The Datong volcanic field (DVF) is located in the northern part of the Trans-North China Orogen and above the tailing edge of stagnant Pacific slab (Fig. 2a). It can be classified into southeastern and northwestern parts according to the morphological structures and lava compositions. Volcanism from the southeastern DVF started in the Middle Pleistocene (0·74 Ma) (Zhao *et al.*, 2015; Sun *et al.*, 2019) and is mainly characterized by lava flows distributed along the Sanggan River fault with a thickness of 3–25 m (Figs 3 and 4a). Basalts erupted in this area show porphyritic textures of olivine tholeiites with the occurrence of olivine, plagioclase and clinopyroxene as phenocrysts, which are set in a groundmass made of plagioclase, clinopyroxene and needle-shaped Fe–Ti oxide (Fig. 4c and e). The northwestern DVF includes at least 17 volcanic cones with eruption ages of as early as 0·4 Ma (Fig. 4b; Zhao *et al.*, 2015; Sun *et al.*, 2019). Olivine phenocrysts are observed in the northwestern DVF basalts with a fine-grained groundmass composed of plagioclase, clinopyroxene and Fe-Ti oxide (Fig. 4d and f). A total of 19 fresh samples including 11 from the southeastern DVF and 8 from the northwestern DVF were collected in this study.

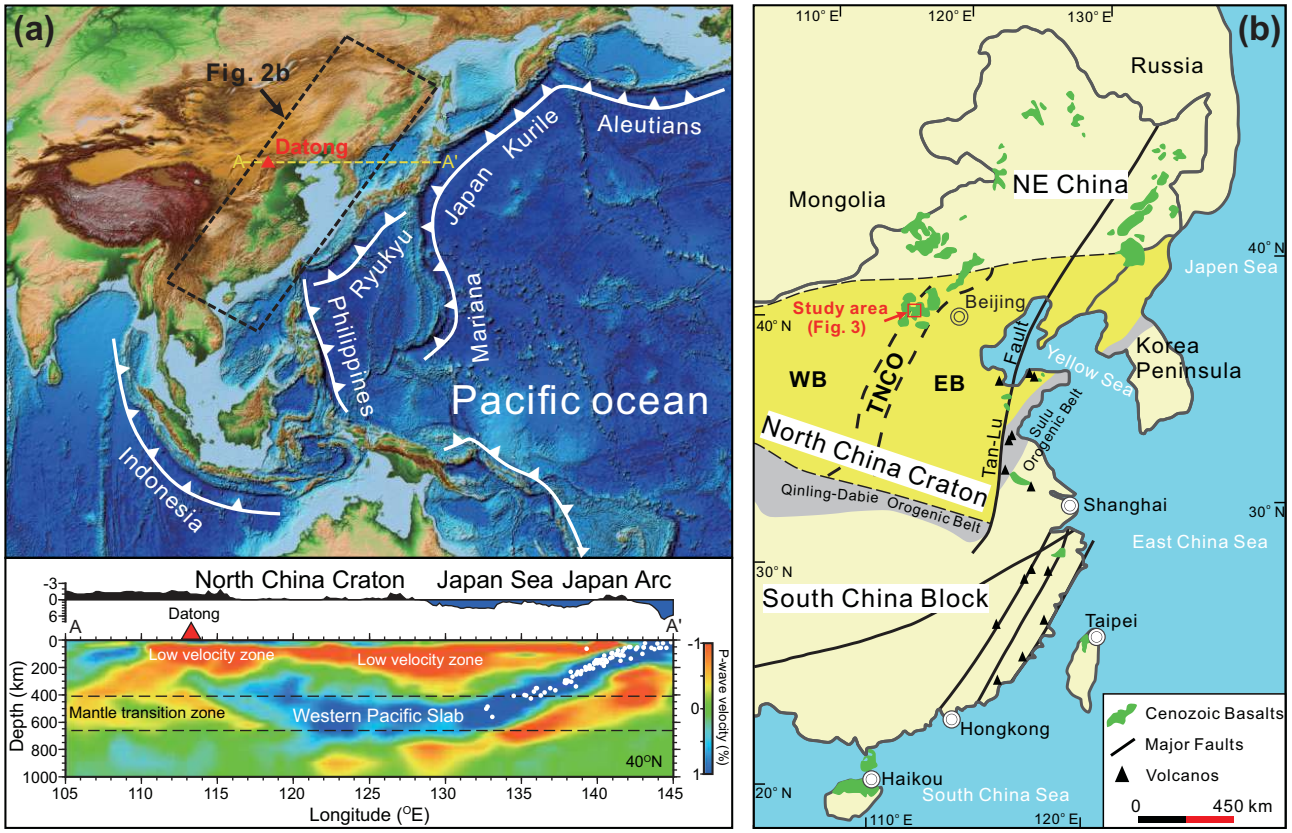

Fig. 2. (a) Topographic map of the western Circum-Pacific region and vertical cross-section of P-wave tomography along the A–A' profile (after Liu *et al.*, 2017*c*). (b) Schematic map showing the major tectonic units of eastern China and the distribution of <110 Ma intraplate basalts (after Liu *et al.*, 2016). TNCO, Trans-North China Orogen; EB, Eastern Block; WB, Western Block.

METHODS

The rock specimens were first sawed into small slices and only the freshest pieces without xenocrysts were handpicked under a binocular scope. Afterwards, the handpicked rock fragments were cleaned with Milli-Q water in an ultrasonic bath and dried down in an oven at 60°C. The cleaned fragments were ground into powders in an agate mortar. Around 30 mg whole-rock powder was fused with ~170 mg $LiBO_2$ in a muffle furnace for one hour and was then quenched. The quenched glass was dissolved in 1 ml of concentrated HNO_3 and diluted to 60 ml by Milli-Q water prior to major element analysis using Leeman Prodigy inductively coupled plasma optical emission spectroscopy (ICP-OES) at the China University of Geosciences, Beijing (CUGB). Loss on ignition (LOI) was determined via calculating the relative mass loss before and after heating ~1 g whole-rock power at ~1000 °C in a muffle furnace for ~30 min. The uncertainties are better than 1% and 2% for elements with contents of >1 wt % and <1 wt %, respectively. For trace element analysis, ~40 mg whole-rock powders were digested in a mixture of concentrated HNO_3 and HCl at 190 °C using Teflon bombs. The dissolved samples were then dried down, redissolved in 1 ml of concentrated HNO_3, and diluted to 80 ml by Milli-Q water. Trace elements were analysed by an

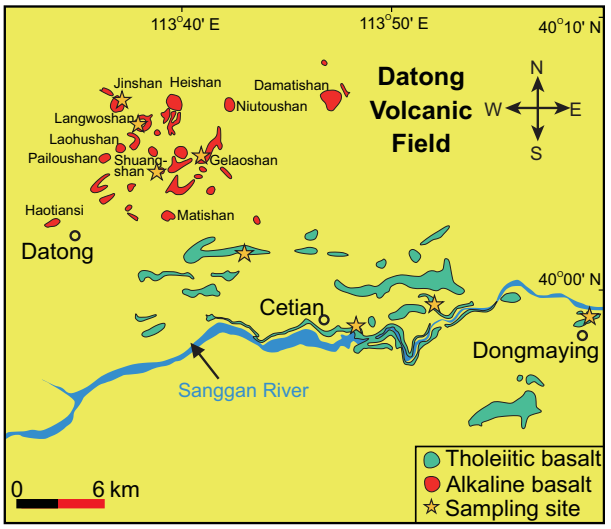

Fig. 3. Distribution of Quaternary basalts in the Datong volcanic field and sampling locations (after Xu *et al.*, 2005). Tholeiitic basalts are mainly distributed along the Sanggan River Fault, while alkaline basaltic volcanism occurs predominantly in the northwestern part of the Datong volcanic field.

Agilent 7500a inductively coupled plasma-mass spectrometer (ICP-MS) at the CUGB. The reproducibility is better than 5% for elements with concentrations of >

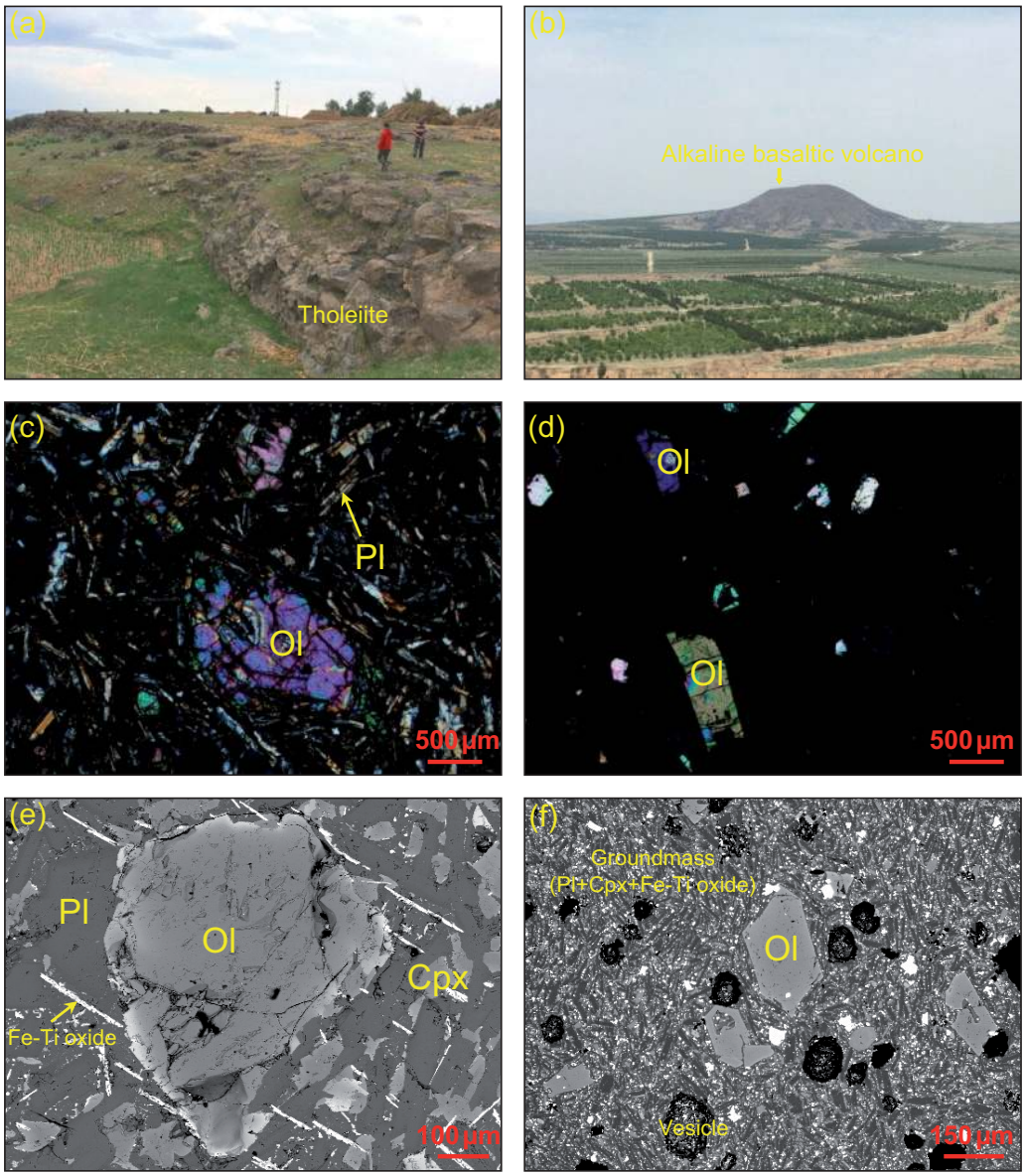

Fig. 4. (a–b) Field photographs showing the outcrops of (a) tholeiitic and (b) alkaline basalts in the Datong volcanic field. (c–d) Microphotography of (c) tholeiitic and (d) alkaline basalts (cross-polarized light). (e–f) Back-scattered electron (BSE) images of (e) tholeiitic and (f) alkaline basalts. Ol, olivine; Cpx, clinopyroxene; Pl, plagioclase.

10 ppb and 10% for those with concentrations of < 10 ppb based on repeated analysis of rock standards. The results of two rock standards GBW017105 and BHVO-2 analysed in this study agree well the recommended values (Supplementary Data Table S1).

A split of the same powders used for major and trace element analysis were digested in a 3:1 concentrated HF: HNO_3 mixture at 150°C in the Savillex® PFA beakers. Following complete dissolution, all samples were evaporated to dryness and then treated with *aqua regia* at 80°C and concentrated HCl at 120°C, respectively, in order to remove any remaining fluorides. After evaporation to dryness, the residues were redissolved in 1 ml of 2·5 N HCl before chromatography. Separation of Sr and rare earth elements (REE) from other matrix elements was achieved by passing through a column loaded with AG50W-X12 (200–400 mesh) resin. A second column loaded with LN resin was used to further separate Nd from other REE. The Sr and Nd isotopic ratios were measured by a Thermo Scientific® *Neptune Plus* multi-collector inductively coupled plasma mass spectrometer (MC-ICP-MS) at the Isotope Geochemistry Lab of the CUGB. The instrumental mass fractionation was calibrated using the exponential law at $^{86}Sr/^{88}Sr = 0{\cdot}1194$ and $^{146}Nd/^{144}Nd = 0{\cdot}7219$. Data were further corrected to a NIST SRM 987 value of $^{87}Sr/^{86}Sr = 0{\cdot}71027$ and an Alfa Nd value of $^{143}Nd/^{144}Nd = 0{\cdot}512425$. A USGS basalt standard BCR-2, processed along the studied samples to monitor accuracy and precision, yielded $^{87}Sr/^{86}Sr = 0{\cdot}704950 \pm 0{\cdot}000014$ and

$^{143}Nd/^{144}Nd = 0{\cdot}512610 \pm 0{\cdot}000008$, which agree well with the values recommended by the GeoReM database ($^{87}Sr/^{86}Sr = 0{\cdot}70493 \pm 0{\cdot}00055$ and $^{143}Nd/^{144}Nd = 0{\cdot}512635 \pm 0{\cdot}000029$; https://georemmpch-mainz.gwdg.de).

Magnesium and zinc isotope analyses were performed after the previous protocols (Liu *et al.*, 2014, 2016; Ke *et al.*, 2016; Gao *et al.*, 2019). Sample digestion follows the same procedure as for Sr and Nd isotopic analysis. After complete dissolution and evaporation to dryness, 1 ml of 1 N HNO_3 or 8 N HCl was added to the dry residue in preparation for Mg or Zn chromatographic purification, respectively. Magnesium and zinc was separated from the matrix elements using 2 ml of cation exchange resin AG50W-X8 and 1 ml of anion exchange resin AG1-X8, respectively. The column chromatographic procedures were performed twice in order to remove the matrix elements utterly with recoveries of both Mg and Zn higher than 99% and a total procedural blank containing less than 10 ng Mg and 6 ng Zn, which account for negligible portions of the loaded Mg and Zn (<0·1% and <0·6%, respectively).

The Mg and Zn isotopic ratios were also determined on a Thermo Scientific® *Neptune Plus* MC-ICP-MS at the Isotope Geochemistry Lab of the CUGB. The measurement was conducted in a low resolution mode under wet plasma conditions. Purified samples dissolved in 3% HNO_3 were introduced into the plasma using a Cetac® ASX-10 autosampler with an uptake rate of 50–100 μl/min. Around 7 V signal of ^{24}Mg and 3 V signal of ^{64}Zn for a standard $10^{11}\Omega$ amplifier were obtained for a solution containing 400 ppb Mg and 200 ppb Zn, respectively. Each measurement constituted one block of 40 cycles with ~4 seconds of integration time and at least three times of independent measurements on the same purified solution were performed for each sample. Instrumental mass bias was corrected by using a standard-sample bracketing (SSB) method for Mg isotopes and a combined SSB and Cu-doping method for Zn isotopes. An extra 100 ppb of Cu was added into each sample and standard Zn solution as the external element for mass bias calibration of Zn isotopes, which is modified after Maréchal *et al.* (1999). The results are reported relative to Mg standard DSM-3 and Zn standard Lyon JMC 3–0749 L in delta (δ) notation:

$$\delta^{26,\,25}\mathrm{Mg}\ (‰) = \left[\frac{\left(^{26,\,25}\mathrm{Mg}/^{24}\mathrm{Mg}\right)_{\mathrm{sample}}}{\left(^{26,\,25}\mathrm{Mg}/^{24}\mathrm{Mg}\right)_{\mathrm{DSM3}}} - 1\right] \times 1000;$$

$$\delta^{66,\,68}\mathrm{Zn}\ (‰) = \left[\frac{\left(^{66,\,68}\mathrm{Zn}/^{64}\mathrm{Zn}\right)_{\mathrm{sample}}}{\left(^{66,\,68}\mathrm{Zn}/^{64}\mathrm{Zn}\right)_{\mathrm{Lyon\ JMC\ 3-0749L}}} - 1\right] \times 1000$$

Long-term external reproducibilities (2SD) of ±0·06‰ for $\delta^{26}Mg$ (Gao *et al.*, 2019) and of ±0·04‰ for $\delta^{66}Zn$ (Wang *et al.*, 2017*b*) were routinely obtained based on repeated analyses of synthetic solutions (e.g. GSB-Mg, IRMM 3702-Zn) and international rock standards (e.g. BHVO-2). The BCR-2 analysed during the course of this study yielded $\delta^{26}Mg = -0{\cdot}14 \pm 0.06‰$ and $\delta^{66}Zn = 0{\cdot}25 \pm 0{\cdot}04‰$, which are in good agreement with the values reported in literature (e.g. An *et al.*, 2014; Chen *et al.*, 2015; Sossi *et al.*, 2015; Teng *et al.*, 2015). The uncertainties of $\delta^{26}Mg$ and $\delta^{66}Zn$ for all samples are given as long-term external reproducibilities (2SD) throughout the text.

RESULTS

Major and trace element geochemistry

The major and trace element data for the Datong basalts are presented in Table 1. The studied samples have very low LOI contents of -0·59 wt % to 0·30 wt %, confirming limited post-eruption low-temperature alteration. In the total alkali vs silica diagram (Le Bas *et al.*, 1986), they can be classified into tholeiitic and alkaline groups (Fig. 5a). Samples from the southeastern DVF belong to tholeiitic basalt and basaltic andesite, while those from the northwestern DVF are alkaline trachybasalt and basanite. We use the more general classification of tholeiitic and alkaline basalts for the two groups of lavas, hereafter. Compared with tholeiitic basalts, alkaline basalts display a wider range of major element contents and have lower SiO_2 and higher Na_2O, K_2O, TFe_2O_3, TiO_2 and P_2O_5 contents (Figs 5 and 6). Alkaline and tholeiitic basalts together exhibit good correlations between SiO_2 and Na_2O+K_2O, TFe_2O_3, TiO_2 and P_2O_5 (Fig. 5), while no obvious correlations exist between MgO and other oxides except that Al_2O_3 and CaO are well correlated with MgO in alkaline basalts (Fig. 6).

Both alkaline basalts and tholeiites display OIB-like trace element patterns in the primitive mantle-normalized trace element diagram (e.g. positive Nb-Ta anomalies, negative Pb anomaly), but the highly incompatible trace element (e.g. Rb, Th, Nb and Zr) abundances of alkaline basalts are much higher than those of tholeiitic basalts (Fig. 7a). The degree of fractionation between light REE and heavy REE is also higher in alkaline basalts (e.g. $La_N/Yb_N = 14{\cdot}6–23{\cdot}0$, $Sm_N/Yb_N = 4{\cdot}67–6{\cdot}53$; N-chondrite normalized, McDonough & Sun, 1995) than in tholeiitic basalts (e.g. $La_N/Yb_N = 4{\cdot}2–9{\cdot}4$, $Sm_N/Yb_N = 2{\cdot}52–3{\cdot}69$) (Fig. 7b).

Sr–Nd–Mg–Zn isotopic compositions

The Sr, Nd, Mg and Zn isotopic data are presented in Table 2. The Sr and Nd isotopic variations of the Datong basalts fall within the scope of OIB, ranging from HIMU-like to EM1-like (Fig. 8a). Alkaline basalts have $^{87}Sr/^{86}Sr$ (0·703220 to 0·703873) lower than and $^{143}Nd/^{144}Nd$ (0·512889 to 0·512959) higher than tholeiitic basalts (0·703891 to 0·704669 and 0·512658 to 0·512823, respectively) and the two groups together define a negative correlation. Similar isotopic characteristics have been commonly observed in Cenozoic basalts from

Table 1: Major (in wt %) and trace (in μg/g) element chemistry of the Datong basalts.

Sample No.	17CT01	17CT03	17CT04	17CT06	17CT08	17CT09	17YG01	17YG02	17YG04	17YG06
Rock type	Tholeiite	Tholeiite	Tholeiite	Tholeiite	Tholeiite	Tholeiite	Tholeiite	Tholeiite	Tholeiite	Tholeiite
SiO_2	52·55	51·87	51·63	51·94	52·29	52·31	52·50	52·10	52·15	53·19
TiO_2	2·12	2·05	2·07	2·10	2·19	2·13	1·77	1·76	1·81	1·95
Al_2O_3	14·14	14·03	13·95	13·88	13·67	13·81	14·26	14·26	14·19	14·24
TFe_2O_3	11·86	11·75	11·85	11·70	12·09	12·09	12·01	12·03	12·17	12·28
MnO	0·15	0·15	0·15	0·14	0·15	0·15	0·14	0·15	0·15	0·15
MgO	6·87	7·12	7·11	6·90	6·88	7·20	6·97	7·13	7·14	6·28
CaO	7·86	7·99	7·94	7·94	7·87	7·92	8·26	8·29	8·16	8·41
Na_2O	3·49	3·54	3·52	3·50	3·34	3·37	3·19	3·17	3·19	3·28
K_2O	0·97	0·98	0·97	0·98	0·79	0·79	0·65	0·70	0·59	0·64
P_2O_5	0·24	0·23	0·26	0·33	0·24	0·23	0·15	0·14	0·16	0·17
LOI	−0·10	−0·19	−0·22	−0·02	−0·19	−0·22	−0·45	−0·15	−0·37	−0·36
Total	100·15	99·52	99·23	99·39	99·31	99·78	99·43	99·58	99·34	100·22
Mg#	0·58	0·59	0·59	0·58	0·57	0·58	0·58	0·58	0·58	0·55
Cr	253·60	256·40	249·20	241·80	242·20	262·60	279·60	271·60	265·40	254·00
Ni	166·48	172·02	170·84	159·14	172·16	186·34	182·26	195·62	161·24	130·56
Zn	103·86	109·72	107·09	109·03	107·24	110·11	97·87	98·43	96·00	99·22
Rb	12·86	12·95	13·40	12·68	11·86	11·48	8·51	8·28	7·97	8·79
Sr	375·20	368·20	373·00	372·80	345·00	340·80	259·20	258·80	255·60	254·40
Y	23·92	23·18	23·30	22·80	24·68	23·86	22·40	22·52	22·82	24·26
Zr	207·60	202·40	201·60	206·00	196·82	188·16	106·72	107·62	105·86	112·90
Nb	28·56	27·72	28·44	28·44	23·30	22·60	11·73	11·90	11·70	12·43
Cs	0·22	0·21	0·22	0·22	0·21	0·21	0·08	0·08	0·08	0·10
Ba	194·16	188·94	190·28	285·00	196·48	193·18	179·59	171·95	160·71	166·87
La	15·96	15·36	15·53	15·25	14·52	14·06	9·57	9·43	9·03	9·58
Ce	33·53	32·22	32·75	32·45	31·60	30·57	20·24	20·19	19·42	20·48
Pr	4·28	4·13	4·19	4·11	4·15	4·01	2·69	2·69	2·58	2·74
Nd	18·23	17·62	17·66	17·53	18·02	17·49	11·58	11·66	11·35	12·01
Sm	4·98	4·83	4·81	4·82	5·06	4·90	3·55	3·57	3·53	3·73
Eu	1·71	1·68	1·65	1·66	1·72	1·70	1·21	1·22	1·22	1·27
Gd	5·63	5·49	5·39	5·36	5·73	5·60	4·08	4·10	4·16	4·37
Tb	0·85	0·82	0·81	0·82	0·87	0·85	0·62	0·63	0·63	0·67
Dy	5·10	5·01	4·92	4·91	5·18	5·08	3·78	3·79	3·86	4·06
Ho	0·97	0·95	0·94	0·93	0·99	0·97	0·73	0·73	0·74	0·78
Er	2·55	2·44	2·40	2·42	2·54	2·50	1·88	1·89	1·91	2·01
Tm	0·34	0·33	0·32	0·32	0·34	0·33	0·25	0·26	0·26	0·27
Yb	2·00	1·95	1·92	1·92	2·02	1·97	1·49	1·50	1·52	1·59
Lu	0·29	0·29	0·28	0·28	0·30	0·29	0·21	0·21	0·22	0·23
Hf	4·96	4·83	4·76	4·80	4·72	4·63	2·43	2·64	2·64	2·76
Ta	1·95	1·88	1·82	1·88	1·43	1·44	0·71	0·68	0·68	0·71
Pb	2·06	2·08	1·86	1·99	1·83	1·91	1·09	1·23	0·99	1·06
Th	2·23	2·17	2·14	2·06	1·78	1·80	0·78	0·78	0·77	0·82
U	0·64	0·64	0·64	0·62	0·52	0·52	0·24	0·24	0·24	0·25

(continued)

Table 1: Continued.

Sample No.	17DT18	17DT01	17DT02	17DT05	17DT06	17DT07	17DT16	17DT17	17GLS03
Rock type	Tholeiite	Alkaline basalt	Alkaline basalt	Alkaline basalt	Alkaline basalt	Alkaline basalt	Alkaline basalt	Alkaline basalt	Alkaline basalt
SiO_2	51·62	48·25	47·31	45·09	48·25	48·12	45·02	45·20	48·03
TiO_2	1·96	2·64	2·75	2·93	2·66	2·64	3·11	3·00	2·51
Al_2O_3	14·69	14·88	14·79	13·90	13·99	13·92	13·88	13·88	13·78
TFe_2O_3	11·49	13·26	13·51	13·97	13·25	13·14	14·48	14·50	13·40
MnO	0·14	0·16	0·17	0·18	0·17	0·17	0·18	0·19	0·17
MgO	6·48	6·17	6·14	7·83	7·35	7·34	7·80	7·72	8·20
CaO	8·08	6·76	6·85	7·89	7·81	7·95	8·02	7·63	8·58
Na_2O	3·59	4·48	4·71	4·35	3·80	3·82	4·55	4·41	3·79
K_2O	1·08	2·65	2·63	2·50	1·77	1·77	1·61	2·50	1·67
P_2O_5	0·32	0·90	0·97	1·00	0·75	0·71	0·94	1·05	0·67
LOI	−0·08	−0·26	−0·59	0·30	−0·42	−0·18	0·24	0·21	−0·44
Total	99·37	99·90	99·24	99·94	99·38	99·40	99·84	100·29	100·36
Mg#	0·57	0·52	0·52	0·57	0·57	0·57	0·56	0·56	0·59
Cr	231·00	144·66	131·86	241·40	256·20	245·20	211·00	221·00	277·20
Ni	170·14	133·84	131·40	199·34	202·80	191·58	188·60	189·58	219·20
Zn	101·72	135·36	144·27	136·89	124·39	123·00	134·75	146·98	121·91
Rb	14·14	41·08	42·42	40·30	27·44	26·68	29·10	41·32	28·10
Sr	392·80	825·00	834·60	837·40	691·40	680·80	845·60	827·40	628·40
Y	22·40	27·58	27·08	28·00	29·22	28·44	27·62	27·74	27·58
Zr	163·34	324·20	325·80	339·20	292·00	283·80	325·00	331·60	266·40
Nb	28·20	75·96	78·10	88·60	62·16	59·64	83·90	85·68	58·66
Cs	0·16	0·47	0·48	0·50	0·33	0·32	0·47	0·52	0·34
Ba	229·46	536·58	557·26	490·82	412·50	406·78	522·72	505·12	372·24
La	18·00	43·17	44·14	48·16	36·73	35·28	46·05	47·56	33·72
Ce	35·60	86·04	87·49	94·00	74·59	69·41	92·25	93·43	67·69
Pr	4·41	10·28	10·53	11·22	8·88	8·46	10·97	11·24	8·09
Nd	17·48	38·80	39·54	41·52	33·88	32·27	40·92	41·61	30·54
Sm	4·57	8·49	8·64	8·73	7·77	7·45	8·74	8·76	7·01
Eu	1·47	2·54	2·56	2·58	2·35	2·26	2·59	2·57	2·12
Gd	4·61	7·43	7·45	7·49	7·06	6·82	7·48	7·48	6·37
Tb	0·66	0·97	0·96	0·97	0·95	0·93	0·98	0·97	0·88
Dy	3·83	5·14	5·06	5·21	5·25	5·10	5·15	5·12	4·80
Ho	0·72	0·90	0·88	0·92	0·95	0·92	0·90	0·90	0·88
Er	1·80	2·15	2·09	2·20	2·35	2·26	2·13	2·13	2·18
Tm	0·24	0·27	0·26	0·28	0·30	0·29	0·26	0·26	0·28
Yb	1·35	1·51	1·45	1·54	1·73	1·67	1·45	1·46	1·63
Lu	0·19	0·21	0·20	0·21	0·24	0·23	0·19	0·19	0·23
Hf	3·98	7·45	7·47	7·69	6·82	6·59	7·33	7·32	5·86
Ta	1·62	4·25	4·30	5·03	3·49	3·42	4·62	4·85	3·47
Pb	1·51	2·70	2·70	2·97	2·40	2·14	3·06	2·68	1·91
Th	1·87	4·39	4·38	5·08	3·66	3·55	4·64	4·73	3·46
U	0·50	1·29	1·31	1·55	1·03	1·02	1·18	1·43	0·99

Mg# = molar ratio of Mg/(Mg+0·85*total Fe)

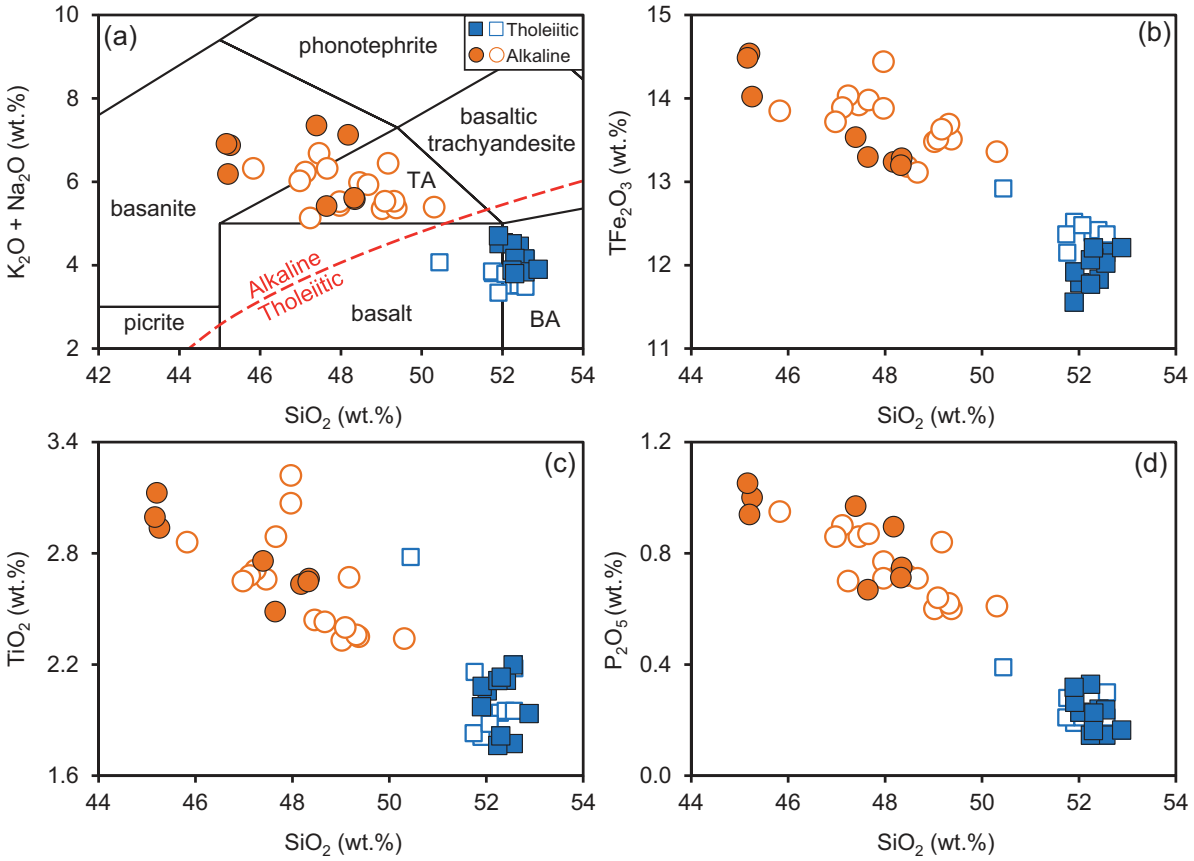

Fig. 5. Covariations of (a) K_2O+Na_2O, (b) TFe_2O_3, (c) TiO_2 and (d) P_2O_5 with SiO_2. The total alkali versus SiO_2 diagram for volcanic classification is after Le Bas *et al.* (1986). The open and solid symbols refer to samples from literature (Xu *et al.*, 2005; Su *et al.*, 2017) and this study, respectively.

other areas of the North China Craton (e.g. Hannuoba, Taihang Mountains, Shandong; Zhi *et al.*, 1990; Tang *et al.*, 2006; Zeng *et al.*, 2011).

The Mg and Zn isotopic compositions of the Datong basalts display an overall range from -0·42‰ to -0·28‰ and from 0·28‰ to 0·46‰, respectively (Figs 9–13), which are in agreement with the previous analyses for Cenozoic basalts from other regions in eastern China for which δ^{26}Mg range from -0·66‰ to -0·23‰ and δ^{66}Zn range from 0·30‰ to 0·63‰ (Liu & Li, 2019 and references therein). The δ^{26}Mg values of Datong alkaline basalts vary from -0·42‰ to -0·38‰ (n = 8), which are lower than the mantle value (-0·25 ± 0·04‰; Teng *et al.*, 2010). Tholeiitic basalts have δ^{26}Mg values ranging from -0·35‰ to -0·28‰ (n = 11), which are higher than those of alkaline basalts and close to the mantle value. Alkaline basalts have δ^{66}Zn values ranging from 0·40‰ to 0·46‰ (n = 8), which are significantly higher than those of the average mantle estimated from non-metasomatized peridotites (0·17 ± 0·08‰, n = 87; Doucet *et al.*, 2016; Wang *et al.*, 2017*b*; Huang *et al.*, 2018*a*, 2019; Sossi *et al.*, 2018; Liu *et al.*, 2019) and average MORB (0·27 ± 0·06‰, n = 13; Wang *et al.*, 2017*b*; Huang *et al.*, 2018*b*). The δ^{66}Zn values of tholeiitic basalts (0·28‰ to 0·37‰, n = 11) are intermediate between alkaline basalts and MORB. Taken together, alkaline and tholeiitic basalts together display trends of increase in δ^{26}Mg and decrease in δ^{66}Zn with decreasing alkalinity (Fig. 9).

DISCUSSION

Origin of low δ^{26}Mg and high δ^{66}Zn of the Datong alkaline basalts

Magmatic processes

Magnesium isotope fractionation during basaltic differentiation is negligible, which is indicated by the indistinguishable Mg isotopic compositions of cogenetic basalts with diverse degrees of differentiation (e.g. MgO varying from 2·37 wt % to 26·87 wt %; Teng *et al.*, 2007). There is a lack of correlation between δ^{26}Mg and SiO_2 or MgO in the Datong basalts (Fig. 10a and b), further suggesting that variation in δ^{26}Mg is unlikely to be a result of magmatic differentiation. A recent study proposed that magnesian chromite crystallization may shift the δ^{26}Mg of differentiated lavas towards lower values (Su *et al.*, 2019). However, no chromite phenocrysts or inclusions are found in the Datong basalts, and there is no correlation between δ^{26}Mg value and Cr concentration (Fig. 10c), excluding the possibility of chromite fractionation. It has been suggested that a maximum Zn

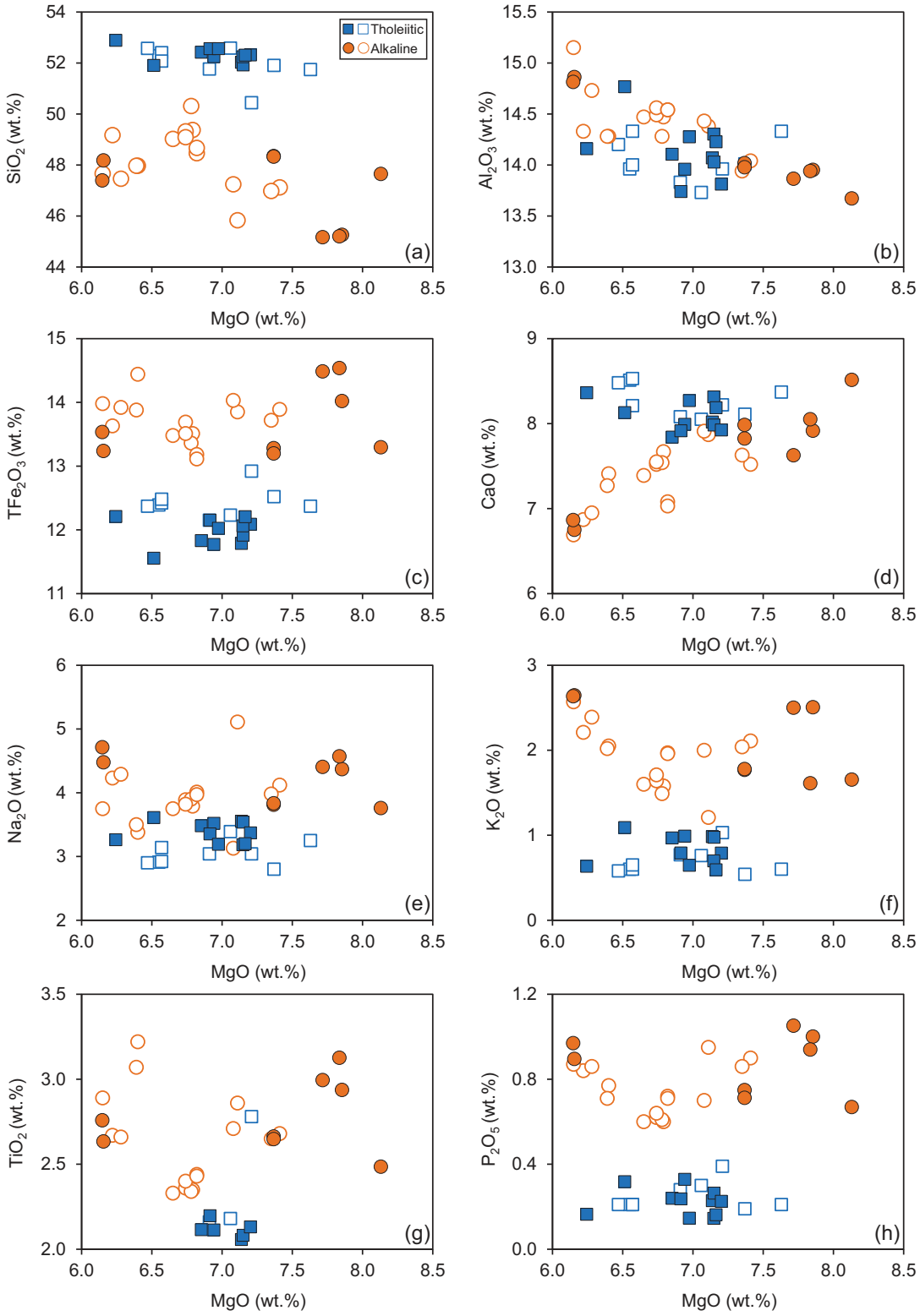

Fig. 6. Covariations of (a) SiO_2, (b) Al_2O_3, (c) TFe_2O_3, (d) CaO, (e) Na_2O, (f) K_2O, (g) TiO_2 and (h) P_2O_5 with MgO. Symbols as in Fig. 5.

isotope fractionation of ~0·1‰ occurs during strong fractional crystallization of the Kilauea Iki basalts (Chen *et al.*, 2013) probably due to segregation of isotopically light olivine crystals (McCoy-West *et al.*, 2018; Yang & Liu, 2019). However, the Datong alkaline basalts with higher $\delta^{66}Zn$ have lower SiO_2 contents, which is opposite to a positive correlation expected for differentiation as exemplified by the Kilauea Iki lavas (Fig. 10d).

Moreover, δ^{66}Zn values are not correlated with MgO content (Fig. 10e), and are significantly higher than those of Kilauea Iki lavas at a given Zn concentration (Fig. 10f). These arguments suggest limited influence of fractional crystallization on the δ^{66}Zn of alkaline basalts.

Recent studies put forward possible Mg and Zn isotope fractionation during partial melting of the mantle especially when garnet or spinel occurs as a residual phase, with the melts enriched in lighter Mg and heavier Zn isotopes (Wang *et al.*, 2017*b*; Zhong *et al.*, 2017; Sossi *et al.*, 2018; Stracke *et al.*, 2018). Nevertheless, partial melting modelling predicts that partial melts from a normal peridotitic mantle (δ^{26}Mg = -0·25‰; δ^{66}Zn = 0·18‰), even if they are generated at a very low melting degree (e.g. 0·5%), still have significantly higher δ^{26}Mg (-0·27‰) and lower δ^{66}Zn (0·25‰) relative to the Datong alkaline basalts (Fig. 11). Therefore, the lower δ^{26}Mg and higher δ^{66}Zn values of alkaline basalts relative to the mantle and MORB are unlikely to have been caused by partial melting of a pristine mantle source, but instead indicate the addition of low-δ^{26}Mg and high-δ^{66}Zn components in their sources.

Mantle source

In this section, we explore the recycling of various slab components into the mantle sources as an explanation for the non-mantle-like Mg and Zn isotopic signatures of alkaline basalts. Such a hybridized source may lie in the subcontinental lithospheric mantle (SCLM) metasomatized by fluids/melts generated by slab dehydration at shallow depths or the asthenospheric mantle modified by deep recycling of residual slab components. Both Mg and Zn isotopes experience limited fractionation during prograde dehydration of subducted mafic crust or sediment (Wang *et al.*, 2014; Inglis *et al.*, 2017). Dehydration of subducted serpentinite was proposed to preferentially release fluids with Mg and Zn isotopic compositions heavier than the mantle (Pons *et al.*, 2016; Teng *et al.*, 2016; Debret *et al.*, 2018*b*). Interaction with isotopically heavy fluids with the mantle is, however, inconsistent with the high δ^{66}Zn but low δ^{26}Mg of the Datong alkaline basalts. Compared with subducted silicate components that are dominantly characterized by mantle-like or MORB-like δ^{26}Mg and δ^{66}Zn, marine carbonates have extremely low δ^{26}Mg (down to -5·57‰) and high δ^{66}Zn values (up to 1·61‰) (Fig. 1), serving as the most plausible metasomatic agent. Carbonates may be recycled into shallow mantle depths via dissolution into subduction-zone fluids or partial melting in warm thermal regimes (Frezzotti *et al.*, 2011; Ague & Nicolescu, 2014; Poli, 2015). However, carbonates that are released into subduction-zone fluids or carbonatitic liquids at sub-arc depths are primarily Ca-rich ones (Frezzotti *et al.*, 2011; Pan *et al.*, 2013; Poli, 2015), which are depleted in Mg and Zn and thus have limited influence on δ^{26}Mg and δ^{66}Zn of the sub-arc mantle. This is supported by the lack of light Mg and heavy Zn isotopic signatures in global arc lavas (Teng *et al.*, 2016; Li *et al.*, 2017; Brewer *et al.*, 2018; Huang *et al.*, 2018*b*; Hu *et al.*, 2020; Pang *et al.*, 2020). Thus, a subduction-metasomatized SCLM is not the required high-δ^{66}Zn and low-δ^{26}Mg source.

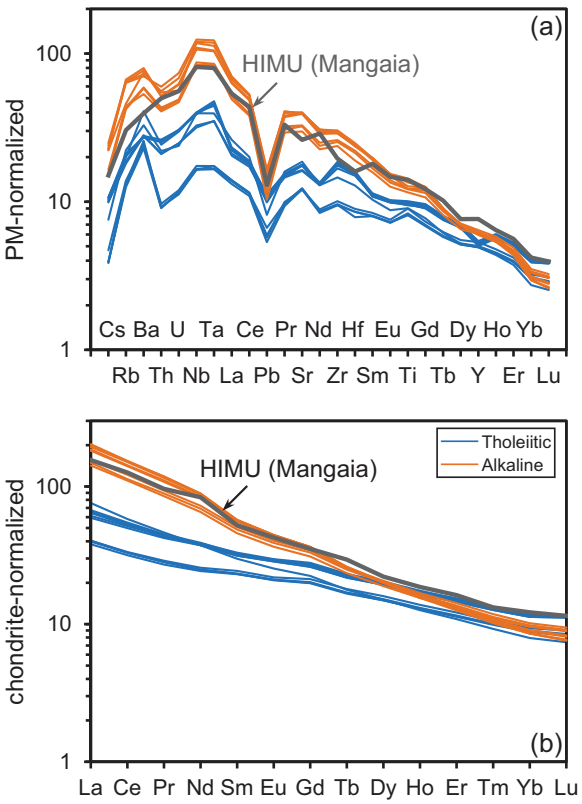

Fig. 7. (a) Primitive mantle (PM)-normalized trace element and (b) chondrite-normalized rare earth element (REE) patterns of the Datong basalts. Patterns of the average Mangaia HIMU basalts are displayed for comparison (Willbold & Stracke, 2006). The PM- and chondrite-normalizing values are from McDonough & Sun (1995).

The Datong alkaline basalts were most likely originated from an asthenospheric mantle source hybridized by carbonated melts derived from deeply subducted oceanic crust, which has also been widely advocated for alkaline basalts with similar Mg and Zn isotopic anomalies from other regions in eastern China (e.g. Liu *et al.*, 2016; Li *et al.*, 2017). Although the fate of carbonates during subduction and the flux of subducted carbon into the convective mantle are still highly uncertain (Kelemen & Manning, 2015; Plank & Manning, 2019), many high-pressure experimental studies and natural observations of high-pressure metamorphic rocks and diamonds suggested that subducted carbonates may survive beyond slab dehydration, particularly during cold subduction (Kerrick & Connolly, 2001; Malusà *et al.*, 2018), and be transported into the mantle beyond sub-arc depths in the form of Mg-rich and Zn-rich species such as dolomite and magnesite (Sato & Katsura, 2001; Frezzotti *et al.*, 2011; Merlini *et al.*, 2012; Li *et al.*, 2014*a*). In addition, a recent study on superdeep diamonds suggests that carbonated mafic oceanic crust, not sediment, is the main carbon-bearing reservoir in

Table 2: Sr–Nd–Mg–Zn isotopic compositions of the Datong basalts

Sample No.	$^{87}Sr/^{86}Sr$ (±2SE)	$^{143}Nd/^{144}Nd$ (±2SE)	$\delta^{25}Mg$ (‰)	2SD (‰)	$\delta^{26}Mg$ (‰)	2SD (‰)	$\delta^{66}Zn$ (‰)	2SD (‰)	$\delta^{68}Zn$ (‰)	2SD (‰)
Tholeiite										
17CT01	0·703913 ± 13	0·512813 ± 9	−0·18	0·05	−0·35	0·06	0·33	0·04	0·66	0·08
17CT03	0·703891 ± 13	0·512820 ± 7	−0·16	0·05	−0·31	0·06	0·36	0·04	0·70	0·08
17CT04	0·703908 ± 13	0·512823 ± 9	−0·17	0·05	−0·32	0·06	0·33	0·04	0·66	0·08
17CT06	0·704229 ± 14	0·512819 ± 10	−0·15	0·05	−0·30	0·06	0·36	0·04	0·71	0·08
17CT08	0·704266 ± 13	0·512803 ± 8	−0·18	0·05	−0·33	0·06	0·34	0·04	0·67	0·08
17CT09	0·704227 ± 14	0·512796 ± 8	−0·17	0·05	−0·32	0·06	0·35	0·04	0·68	0·08
17YG01	0·704591 ± 15	0·512658 ± 8	−0·14	0·05	−0·30	0·06	0·31	0·04	0·60	0·08
17YG02	0·704669 ± 13	0·512688 ± 8	−0·14	0·05	−0·31	0·06	0·28	0·04	0·56	0·08
17YG04	0·704643 ± 12	0·512700 ± 7	−0·14	0·05	−0·29	0·06	0·29	0·04	0·58	0·08
17YG06	0·704551 ± 12	0·512705 ± 9	−0·14	0·05	−0·28	0·06	0·30	0·04	0·59	0·08
17DT18	0·704209 ± 13	0·512786 ± 9	−0·16	0·05	−0·34	0·06	0·37	0·04	0·73	0·08
Alkaline basalt										
17DT01	0·703656 ± 12	0·512937 ± 9	−0·20	0·05	−0·41	0·06	0·44	0·04	0·87	0·08
17DT02	0·703562 ± 15	0·512930 ± 9	−0·23	0·05	−0·42	0·06	0·43	0·04	0·85	0·08
17DT05	0·703220 ± 14	0·512959 ± 9	−0·21	0·05	−0·41	0·06	0·46	0·04	0·91	0·08
17DT06	0·703873 ± 13	0·512889 ± 9	−0·21	0·05	−0·40	0·06	0·42	0·04	0·83	0·08
17DT07	0·703841 ± 14	0·512891 ± 9	−0·19	0·05	−0·38	0·06	0·41	0·04	0·81	0·08
17DT16	0·703725 ± 14	0·512952 ± 10	−0·20	0·05	−0·40	0·06	0·44	0·04	0·87	0·08
17DT17	0·703365 ± 13	–	−0·19	0·05	−0·38	0·06	0·42	0·04	0·85	0·08
17GLS03	0·703686 ± 13	0·512922 ± 8	−0·21	0·05	−0·40	0·06	0·40	0·04	0·79	0·08
Rock standard										
BCR-2	0·704950 ± 14	0·512610 ± 8	−0·08	0·05	−0·14	0·06	0·25	0·04	0·51	0·08

2SE for Sr and Nd isotopic ratios equals two times the standard error of a single measurement containing 180 cycles. Long-term external reproducibilities (2SD) for Mg and Zn isotopic ratios are used in this study.

slabs subducted to the MTZ depths (Regier *et al.*, 2020). This is consistent with the HIMU-like trace elemental and Sr-Nd isotopic characteristics of the Datong alkaline basalts, suggesting recycling of oceanic crust into their mantle sources (Figs 7 and 8). Nevertheless, compared with classic HIMU-type OIBs (e.g. Mangaia) with $^{206}Pb/^{204}Pb > 20·5$ (Stracke *et al.*, 2005), the Datong alkaline basalts and other alkaline basalts from eastern China have less radiogenic Pb isotopic compositions ($^{206}Pb/^{204}Pb$ of up to ~18·5; Basu *et al.*, 1991; Sakuyama *et al.*, 2013; Xu *et al.*, 2018), which are close to those of young HIMU-type OIBs (e.g. Canary, $^{206}Pb/^{204}Pb = 19$–20; Thirlwall, 1997). These features are best explained by a young recycled oceanic crustal component, which is probably derived from the stagnant Pacific slab in the MTZ, as revealed by the spatial coupling of the low-$\delta^{26}Mg$ and high-$\delta^{66}Zn$ alkaline basalts from the whole eastern China and the stagnant Pacific slab (Liu *et al.*, 2016; Li *et al.*, 2017).

Melting experiments suggest that upon reaching the MTZ carbonatitic melts are produced by melting of carbonated oceanic crust (Thomson *et al.*, 2016). Afterwards, carbonatitic melt percolation creates the Mg and Zn isotope heterogeneity in the mantle source of alkaline basalts, and significantly elevates the oxygen fugacity of source region at the same time. The latter is evidenced by the high $\delta^{56}Fe$ (up to 0·29‰; He *et al.*, 2019), unfractionated platinum-group element (PGE) patterns and high total PGE contents (e.g. Ir = 0·25 ± 0·14 ppb; Cai *et al.*, 2021), and high oxygen fugacity (ΔFMQ of up to 1·6; Hong *et al.*, 2020*a*) observed in alkaline basalts from eastern China. Decompression melting of this upwelling carbonated and oxidized mantle domain produced carbonated silicate melts parental to alkaline basalts. Furthermore, the SCLM beneath eastern China was inferred to be oxidized enough to stabilize carbonate or carbonatite since late Mesozoic (Geng *et al.*, 2019; Hong *et al.*, 2020*b*). Therefore, alkaline basalts can be effectively extracted through the SCLM with retaining their strong 'carbonate-like' Mg and Zn isotopic signals (Aulbach, 2018).

Mechanism for alkaline to tholeiitic transition

Fractional crystallization and partial melting

Both tholeiitic and alkaline basalts display no correlation between MgO and most oxides (e.g. SiO_2, Fe_2O_3, Na_2O and K_2O; Fig. 6), indicating that fractional crystallization of mafic minerals (e.g. olivine and pyroxene) is not a possible mechanism for the compositional transition. The exceptions are CaO and Al_2O_3 that are positively correlated with MgO for alkaline basalts (Fig. 6b and d), probably due to the segregation of clinopyroxene. The significant Mg and Zn isotopic differences between alkaline and tholeiitic basalts are also in disagreement with the negligible isotope fractionation during basaltic differentiation as discussed above. By contrast, the $\delta^{26}Mg$ and $\delta^{66}Zn$ of alkaline and tholeiitic basalts are well correlated with the abundances of incompatible trace elements (e.g. Rb, Th, Nb and Zr, R^2=0·85–0·95; Fig. 11), which appears to reflect a melting control on Mg and Zn isotopic variations. However, the changes in $\delta^{26}Mg$ and $\delta^{66}Zn$ values of partial melts induced by 0·5% to 20% melting of a single peridotitic source are no more than ±0·02‰ (Fig. 11), which is fairly smaller than the $\delta^{26}Mg$ and $\delta^{66}Zn$ differences

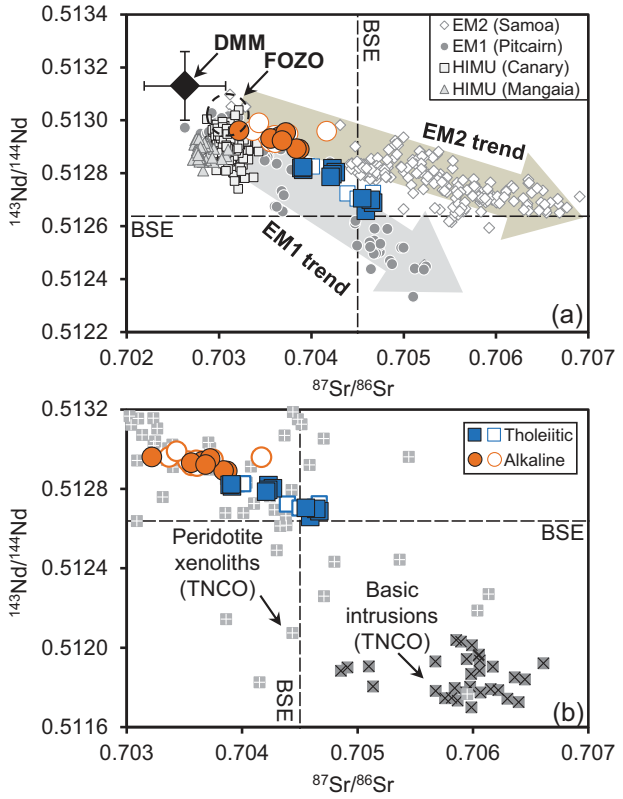

Fig. 8. Plots of $^{143}Nd/^{144}Nd$ vs $^{87}Sr/^{86}Sr$. Symbols as in Fig. 5. Data for OIB from type-localities of EM1, EM2 and HIMU mantle components are from the GeoRoc database (http://georoc.mpch-mainz.gwdg.de/georoc). The average compositions of the BSE (depicted by dashed lines) and the DMM as well as the FOZO field are from Workman & Hart (2005) and Hart *et al.* (1992). Data for peridotite xenoliths from the Trans-North China Orogen (TNCO) are compiled from Song & Frey (1989), Fan *et al.* (2000), Rudnick *et al.* (2004), Tang *et al.* (2008, 2011, 2013) and Liu *et al.* (2012). Data for basic intrusions from the TNCO are from Zhang *et al.* (2004).

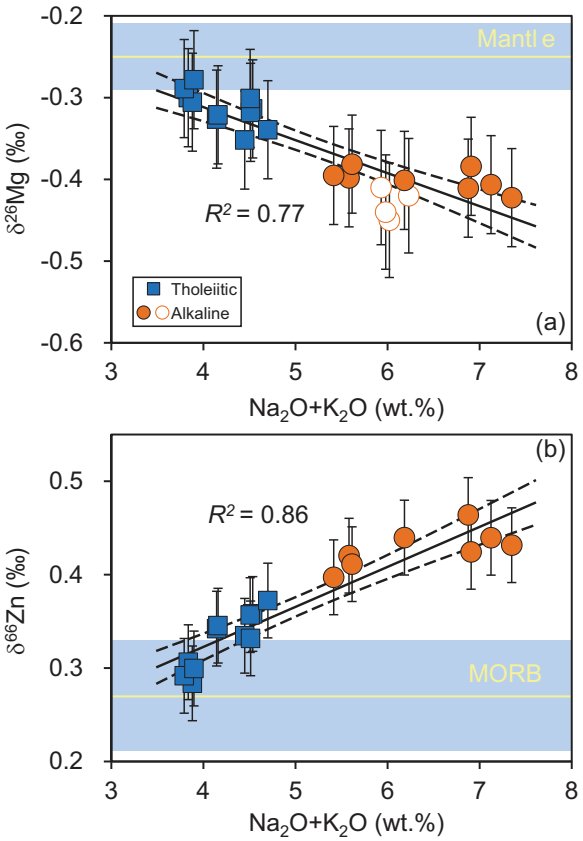

Fig. 9. Covariations of (a) $\delta^{26}Mg$ and (b) $\delta^{66}Zn$ with Na_2O+K_2O. The mantle $\delta^{26}Mg$ ($-0{\cdot}25 \pm 0{\cdot}04$‰) is from Teng (2017). Symbols as in Fig. 5. The MORB $\delta^{66}Zn$ ($0{\cdot}27 \pm 0{\cdot}06$‰; Wang *et al.*, 2017*b*; Huang *et al.*, 2018*b*) instead of the mantle value is plotted for comparison because Zn isotopes can be slightly fractionated during partial melting of the mantle (see text for details). The black solid lines and dashed curves are the best fitting lines and 95% confidence envelopes of linear regression through all samples.

between alkaline and tholeiitic basalts. The magnitude of equilibrium Mg and Zn isotope fractionation between carbonate and silicate phases at mantle temperatures (e.g. 1300° C) is below ±0·04‰ (Macris *et al.*, 2013; Ducher *et al.*, 2016), further indicating that Mg and Zn isotopes also experience limited fractionation during partial melting of carbonated mantle. This suggests that varying degree of partial melting of a single source is unlikely to account for the Mg and Zn isotopic variations in the Datong basalts.

Interaction between carbonated silicate melt and metasomatized lithospheric mantle

The correlations of $\delta^{26}Mg$ and $\delta^{66}Zn$ with incompatible trace element concentrations (Fig. 11) can be generated by mixing of variable proportions of two isotopically and chemically distinct sources, which is supported by the excellent correlations of $\delta^{26}Mg$ and $\delta^{66}Zn$ with $^{87}Sr/^{86}Sr$ and $^{143}Nd/^{144}Nd$ (Fig. 12). One source characterized by lower $\delta^{26}Mg$ and higher $\delta^{66}Zn$ than the mantle is the carbonated mantle source for the alkaline basalts as discussed above. Another source should possess pristine mantle-like $\delta^{26}Mg$ and $\delta^{66}Zn$ values and carry Sr–Nd isotopic affinity of an EM1-type mantle component. The stronger EM1 signature of tholeiitic basalts than alkaline basalts is in contrast to what would be expected in a model of upwelling pyroxenite-bearing peridotite where the higher-volume melts (i.e. tholeiitic basalts) should possess a weaker contribution from enriched components (Sobolev *et al.*, 2007). The enriched Sr and Nd signatures of tholeiitic basalts may be a result of continental crust assimilation, but in this case, the MgO contents of tholeiitic basalts should be lower than those of alkaline basalts, which is in conflict with the overlapping MgO content between the two basalt groups (Fig. 6). The OIB-like trace element characteristics of the Datong tholeiitic basalts (Fig. 7), such as the remarkably negative Pb anomaly in the primitive mantle-normalized trace element diagram, are also against significant crustal assimilation. Ancient sediments subducted to the MTZ have been recently invoked to account for the EM1 isotopic signatures of some Cenozoic basaltic lavas from northeast China (Wang *et al.*, 2017*a*). However, those basalts are

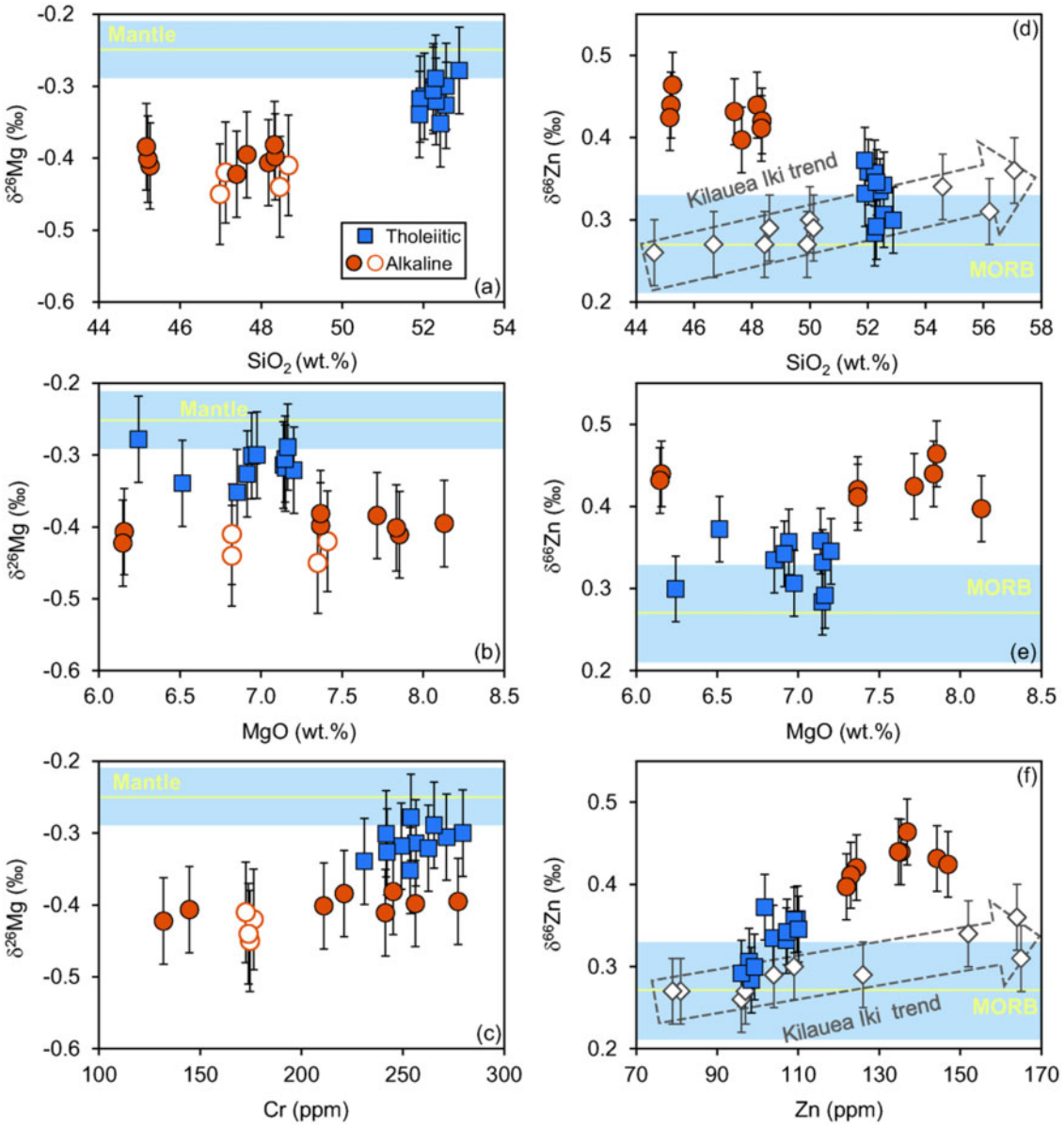

Fig. 10. (a–c) Covariations of δ^{26}Mg with SiO_2, MgO and Cr. (d–f) Covariations of δ^{66}Zn with SiO_2, MgO and Zn. Symbols as in Fig. 5. The Kilauea Iki (Hawaii) lavas (open diamond) that were formed via various extents of magmatic differentiation are also plotted for comparison (Chen *et al.*, 2013).

Note: Figure Replacement Requested.

characterized by extremely high K_2O contents (>3 wt %) and K_2O/Na_2O ratios (>1), in sharp contrast to the low K_2O contents (<1 wt %) and K_2O/Na_2O ratios (<0·3) of the Datong tholeiitic basalts, suggesting a distinct origin for the EM1 source of the Datong basalts.

An EM1 component from the SCLM was previously proposed to have contributed to the formation of weakly alkaline basalts and tholeiites from the North China Craton (Song *et al.*, 1990; Zhi *et al.*, 1990; Basu *et al.*, 1991; Tang *et al.*, 2006). This component is evident in peridotite xenoliths with enriched Sr and Nd isotopic signatures entrained by Cenozoic alkaline basalts from the Trans-North China Orogen (Fig. 8). These peridotites usually have refractory compositions and ancient Re-depletion Os model ages (1·5–3·0 Ga), potentially representing relics of ancient SCLM (Xu *et al.*, 2008; Liu *et al.*, 2012; Tang *et al.*, 2013). The SCLM-derived Mesozoic basic intrusions or basalts from the Trans-North China Orogen are characterized by extremely high $^{87}Sr/^{86}Sr$ (~0·705–0·710) and low $^{143}Nd/^{144}Nd$ (~0·5117–0·5122), which are also indicative of an isotopically enriched SCLM in the study area (Fig. 8) (Zhang *et al.*, 2004). Metasomatism by ancient asthenospheric melts, subduction-zone fluids, sediment melts or delaminated lower continental crust associated with multiple pre-Cenozoic subduction/collision events have been proposed to impart an EM1 isotopic signature to the SCLM beneath the North China Craton (e.g. Zhang *et al.*, 2004;

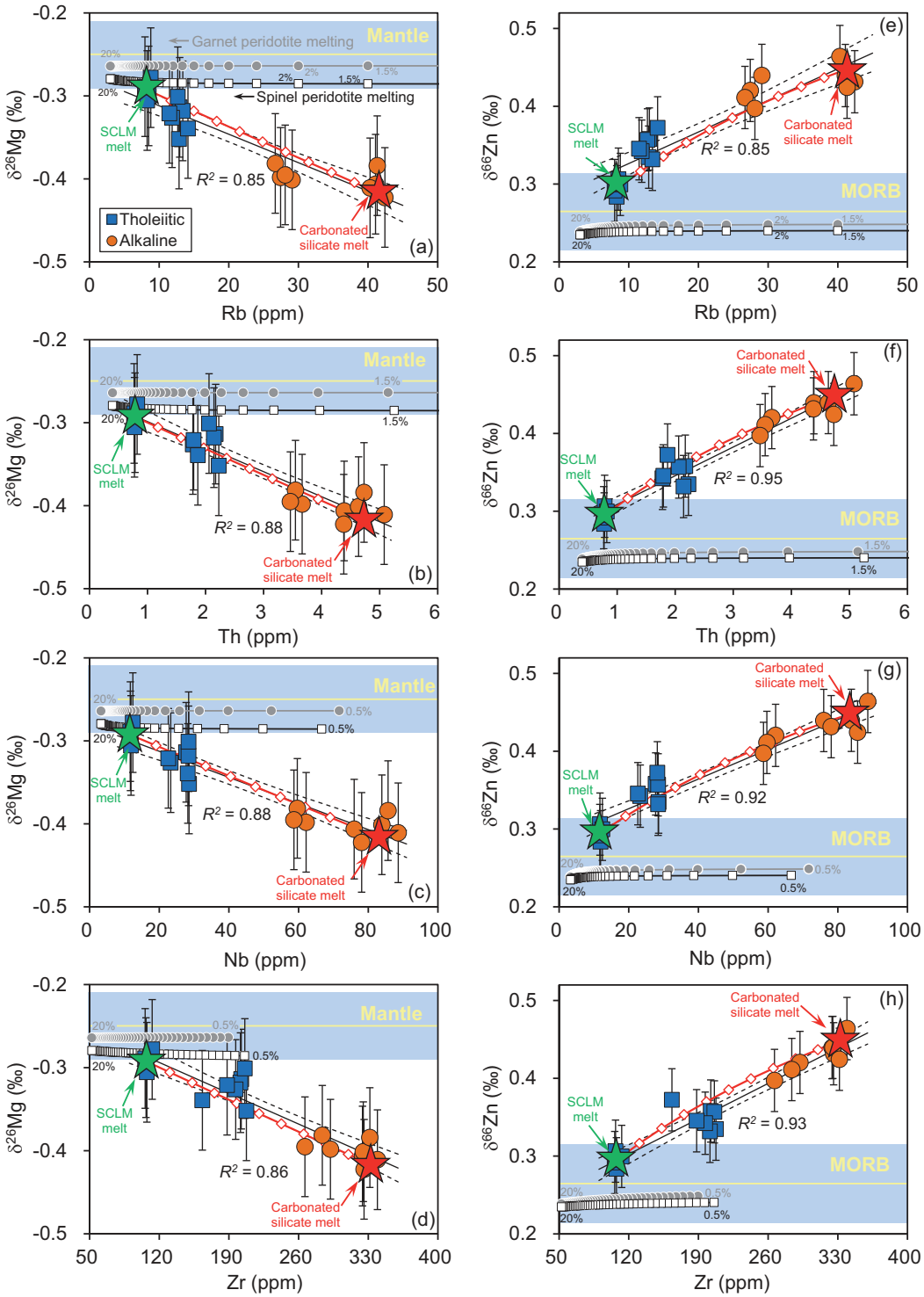

Fig. 11. Covariations of (a–d) δ^{26}Mg or (e–f) δ^{66}Zn with Rb, Th, Nb and Zr. Symbols as in Fig. 5. The black solid lines and dashed curves are the best fitting lines and 95% confidence envelopes of linear regression through all samples. The black and grey curves denote the trends for melts from 0·5%–20% partial melting of spinel-facies and garnet-facies peridotites, respectively. Open squares and grey circles refer to 0·5% increment of non-modal batch melting (modelling details are given in the appendix). The red curves represent mixing of hypothetical carbonated silicate melt with SCLM-derived melt. As an approximation, carbonated silicate melt is given as the mean composition of samples 17DT02 and 17DT05 and SCLM-derived melt is given as the mean composition of samples 17YG01, 17YG02, 17YG04 and 17YG06.

Zheng *et al.*, 2006; Yang & Li, 2008; Tang *et al.*, 2013). However, these metasomatic processes seem to have a week impact on the Mg and Zn isotopic compositions of the SCLM as indicated by mantle-like or MORB-like δ^{26}Mg and δ^{66}Zn values of the SCLM-derived Mesozoic basalts from the North China Craton (Yang *et al.*, 2012;

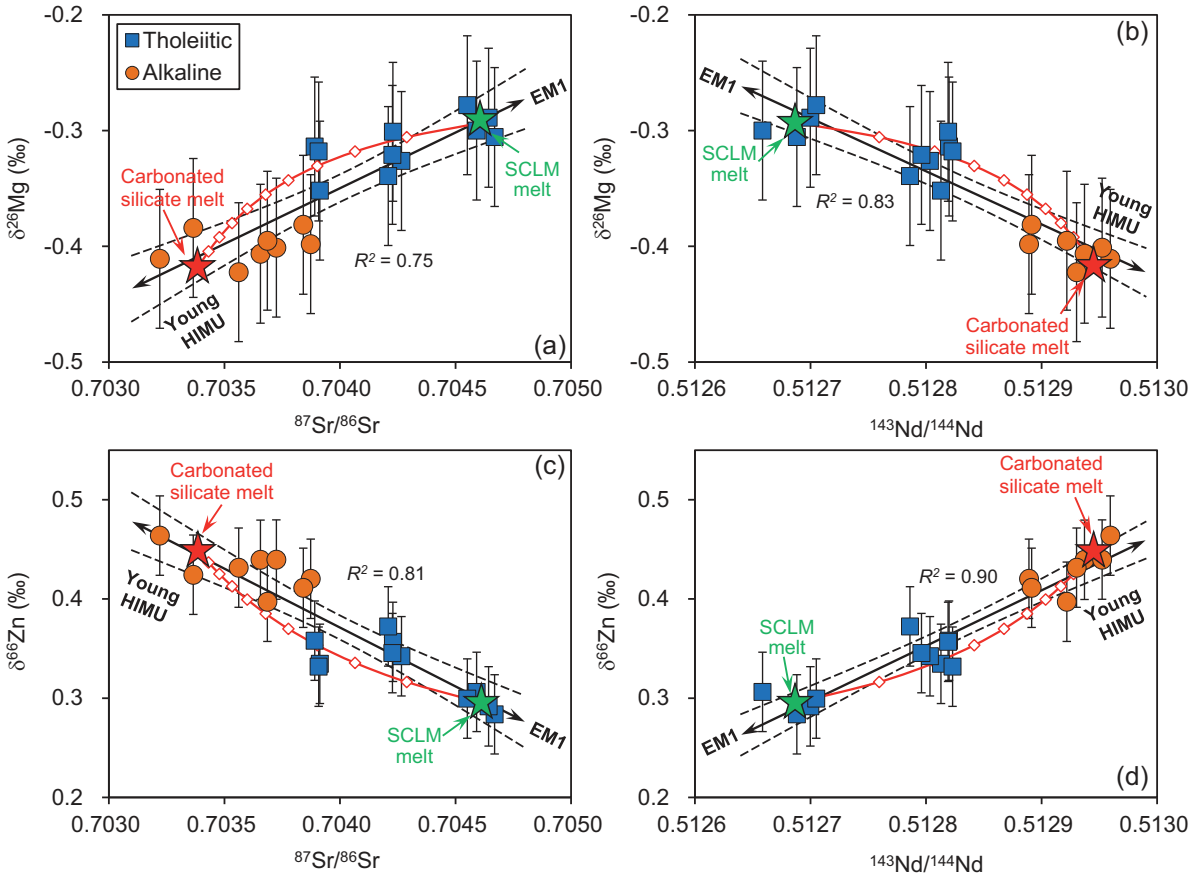

Fig. 12. Covariations of (a–b) δ^{26}Mg or (c–d) δ^{66}Zn with ^{87}Sr/^{86}Sr and ^{143}Nd/^{144}Nd. Symbols as in Fig. 5. The black solid lines and dashed curves are the best fitting lines and 95% confidence envelopes of linear regression through all samples. The red curves represent mixing of hypothetical carbonated silicate melt with SCLM-derived melt. The two assumed endmember melts are the same as in Fig. 11.

Liu *et al.*, 2016; Li *et al.*, 2017; Wang *et al.*, 2017*b*). This may reflect that the EM1-like metasomatic agents are mainly melts or fluids derived from recycled components that have mantle-like Mg and Zn compositions (e.g. siliciclastic sediments) or contain much less Mg and Zn than the SCLM (e.g. Ca-rich carbonates). Therefore, the required EM1 source for the tholeiitic basalts is most likely to be the metasomatized SCLM. Nevertheless, it is unlikely that the Datong tholeiitic basalts are derived from an isotopically heterogeneous SLCM alone since some samples have lighter Mg and heavier Zn isotopic compositions than the mantle, which still requires contribution from a carbonated mantle source. Therefore, the transition from alkaline to tholeiitic basalts is best ascribed to increasing contribution from an isotopically homogenous enriched SCLM during interaction of carbonated silicate melts parental to the alkaline basalts with the SCLM.

Melt-rock or melt-melt interaction?

Previous studies have highlighted carbonated melt metasomatism in the SCLM of eastern China based on petrological and geochemical observations on mantle xenoliths (Xiao *et al.*, 2013; Deng *et al.*, 2017; Zong & Liu, 2018; Lin *et al.*, 2020). During the interaction between melt and lithospheric mantle, the ascending carbonated silica-undersaturated melts may be in disequilibrium with the cooled lithospheric mantle and continuously transform into less silica-undersaturated melts via consumption of orthopyroxene and concomitant crystallization of olivine and clinopyroxene (Dalton & Wood, 1993; Yaxley *et al.*, 1998; Ionov *et al.*, 2005; Russell *et al.*, 2012; Aulbach *et al.*, 2017; Li & Wang, 2018). This process results in transformation of lherzolite or harzburgite into wehrlite, which has been referred to as 'wehrlitization' and been usually recognized in mantle xenolith suites along the Tan-Lu fault belt of eastern China (Xu *et al.*, 1996; Xiao *et al.*, 2013; Lin *et al.*, 2020) as well as in faults or rifts in general (e.g. Aulbach *et al.*, 2020). The Datong tholeiites also occurred along a deep fault (Sanggan River fault), which favors wehrlitization. The wehrlites from the North China Craton are also often characterized by lighter Mg and heavier Zn isotopic compositions than the mantle (Xiao *et al.*, 2013; Wang *et al.*, 2017*b*), consistent with the results of reaction between carbonated silicate melt and the SCLM. We recognize that the realistic melt-SCLM reaction may be more complicated than mixing of melts with just orthopyroxene, given that

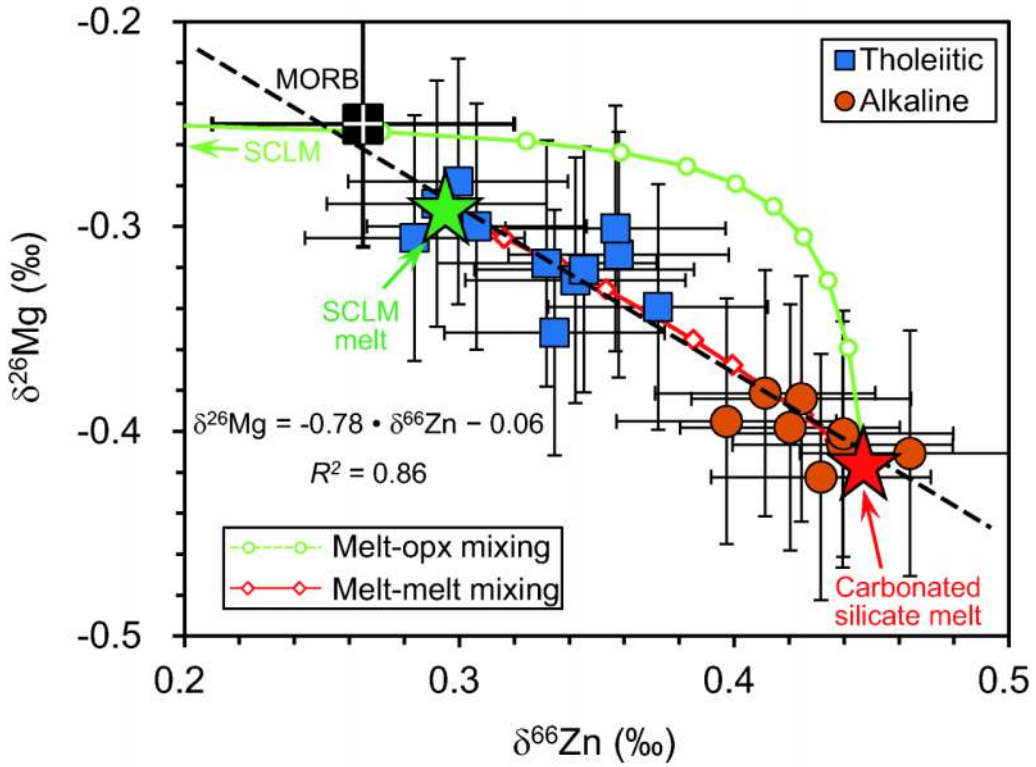

Fig. 13. Plot of δ^{26}Mg against δ^{66}Zn. Symbols as in Fig. 5. The dashed line refers to the best fitting line of linear retrogression through all samples. The green and red curves represent mixing of hypothetical carbonated silicate melt with orthopyroxene (opx) and SCLM-derived melt, respectively. Parameters for the two melt endmembers are the same as in Fig. 11. For the orthopyroxene, MgO (33 wt %) and Zn (30 ppm) concentrations are reasonably assumed according to the data reported in Tang *et al.* (2013) and Wang *et al.* (2017*b*); δ^{26}Mg (-0·25‰) and δ^{66}Zn (0·18‰) are set to be the mean values of mantle peridotite xenoliths from the North China Craton (Teng, 2017; Wang *et al.*, 2017*b*).

Note: Figure Replacement Requested.

amphibole or phlogopite may be precipitated or consumed during this process (e.g. Lin *et al.*, 2020). Nevertheless, these hydrous minerals are subordinate in the SCLM of the North China Craton (<1 vol.%; Xu & Bodinier, 2004; Xiao *et al.*, 2010) and should not play an important role in changing the compositions of reacting melts. In the following, we utilize an Mg–Zn isotope binary mixing model to test whether or not wehrlitization can result in the transition from alkaline to tholeiitic basalts. For simplicity, the most silica-undersaturated alkaline basalt was taken as an approximation to the reacting carbonated silicate melt and the composition of orthopyroxene was reasonably presumed based on data for peridotite xenoliths from the North China Craton reported previously (Tang *et al.*, 2013; Teng, 2017; Wang *et al.*, 2017*b*). The modelling result shows that melt-orthopyroxene reaction yields a hyperbolic trend that observably deviates from the near-linear Mg and Zn isotopic correlations in the Datong basalts due to the striking difference in MgO/Zn concentration ratio between melt (~500) and orthopyroxene (~10 000) (Fig. 13). This suggests that the subsolidus SCLM is unlikely to be directly involved in the interaction process.

Lundstrom (2000) suggested that diffusive infiltration of alkalis into the lithosphere is able to induce its fusion that is chemically, not thermally, driven at typical temperatures of lithospheric mantle. The melts generated at the alkaline basalt-peridotite interface are more enriched in SiO_2 and depleted in MgO than peridotite and thus probably represent the reactant that underwent interaction with the alkaline basalts. Taking the most silica-saturated tholeiitic basalt as an approximation to the reacting SCLM-derived melt, mixing of these two endmember melts can perfectly reproduce the near-linear Mg and Zn isotopic trend and the near-linear correlations of δ^{26}Mg and δ^{66}Zn with incompatible element concentrations, $^{87}Sr/^{86}Sr$ and $^{143}Nd/^{144}Nd$ (Figs 11 and 12). This indicates that the SCLM has undergone partial melting during its interaction with the alkaline basalts. In this scenario, the over-thickened lithospheric keel may have been eroded as advocated by Li & Wang (2018) (Fig. 14). Of note is that tholeiitic basalts are slightly older than alkaline basalts in Datong. This means that melt-SCLM interaction occurred firstly, leading to the formation of tholeiitic basalts and lithospheric thinning. Consequently, a thinned lithosphere may favor the extraction of alkaline basalts afterwards. Lithospheric removal in this way mainly took place in the occurrences of basalts carrying strong EM1 signatures, such as the tholeiitic basalts

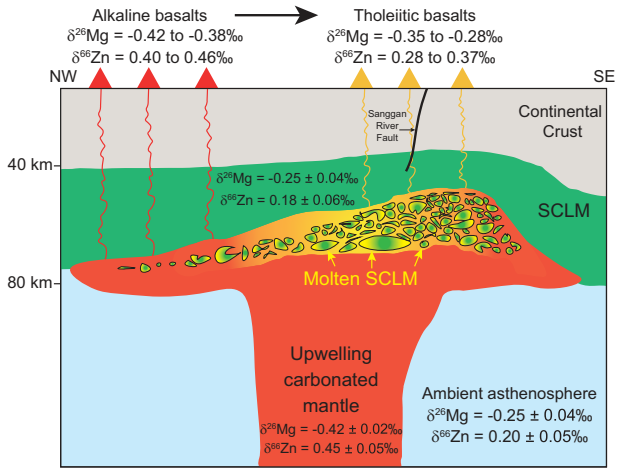

Fig. 14. Schematic model illustrating the transformation from alkaline to tholeiitic basalts via interaction between carbonated silicate melts and the SCLM. Data sources are the same as Fig. 13, except for the asthenospheric mantle that is taken as the mean composition of the DMM (Teng, 2017; Wang *et al.*, 2017*b*).

from the Datong volcanic field and weakly alkaline basalts from Shandong Peninsula (Wang *et al.*, 2018*b*). Interestingly, these high-silica basalts are dominantly distributed along the deep faults (i.e. Sanggan River fault and Tan-Lu fault), where the lithosphere is thinner than surrounding regions where low-silica and strongly alkaline basalts were erupted. Guo *et al.* (2020) recently proposed a 'lid effect' to interpret the compositional variation in intracontinental basalts from eastern China basalts based on correlations between basalt chemistry and lithospheric thickness, that is, melts erupted on thinner lithosphere have geochemical characteristics of higher extent of partial melting compared with melts erupted on thicker lithosphere. However, the strong correlations between Mg–Zn isotopic compositions and basaltic compositions observed in the Datong basalts cannot be simply produced by varying degrees of partial melting of a single source, but require mixing of melts derived from two isotopically distinct mantle sources as discussed above. This suggests a main role of interaction between carbonated silicate melts and SCLM in shifting the compositions of eastern China basalts.

Implications for compositional diversity of intracontinental basalts

The process that is responsible for the alkaline to tholeiitic transition in Datong volcanoes may be considered as one of major mechanisms responsible for the compositional variability of intracontinental basalts from eastern China and other regions. When taking all available data for Cenozoic basalts from the South China Block and North China Craton into account, a broad tendency towards higher δ^{26}Mg and lower δ^{66}Zn values with increasing SiO_2 content and decreasing alkalinity is observed (Fig. 15). This suggests that the compositional transition is accompanied by covariations in Mg and Zn isotopic compositions. Given that Mg and Zn isotopes are insignificantly fractionated during partial melting and high-silica basalts from these areas are often more isotopically enriched than low-silica basalts, we suggest that the melt-SCLM interaction may play an important role in transferring low-silica alkaline basalts into high-silica alkaline and tholeiitic basalts from eastern China, although source heterogeneity and varying degrees of partial melting can also contribute to the compositional variability of these basalts.

Our model may also apply to intracontinental basalts elsewhere. For example, Cenozoic intracontinental volcanism occurring widely within Zealandia and circum-Mediterranean regions exhibits a great range in composition ranging from nephelinitic to tholeiitic (Lustrino & Wilson, 2007; Timm *et al.*, 2010; Brombin *et al.*, 2019). Radiogenic signatures of primitive samples show that low-silica alkaline basalts from the above regions generally have HIMU- or FOZO-like compositions, interpreted as melts derived from partial melting of upwelling asthenosphere hybridized by subducted oceanic crust, whilst many high-silica alkaline and tholeiitic samples often have EM1- or EM2-like compositions and were considered to reflect additional contribution from a metasomatized SCLM (Lustrino & Wilson, 2007; Timm *et al.*, 2010). A preliminary study on alkaline basalts from Antipodes Volcano, Zealandia also revealed low δ^{26}Mg (down to -0·47‰) for these basalts and suggested a carbonated mantle source for these basalts (Wang *et al.*, 2016). In addition, carbonatite or carbonated silicate melt metasomatism has also been suggested to occur within the SCLM in these regions (e.g. Scott *et al.*, 2014; Brombin *et al.*, 2018). These features remarkably resemble those of intraplate basalts from eastern China, implying common origins of these lavas. Future investigations of Mg and Zn isotopic compositions of intracontinental basalts from regions with similar backgrounds can be made to verify this assumption.

CONCLUSIONS

The mechanism responsible for alkaline to tholeiitic transition in intraplate basalts from the Datong volcanic filed, eastern China was explored in this study by combining stable Mg and Zn isotopes with radiogenic Sr and Nd isotopes. Alkaline basalts have young HIMU-like Sr and Nd isotopic compositions and significantly lower δ^{26}Mg and higher δ^{66}Zn than the mantle values, suggesting derivation of these lavas from an asthenospheric mantle source modified by carbonated melts derived from the stagnant Pacific oceanic crust in the MTZ. Tholeiites have MORB-like δ^{26}Mg and δ^{66}Zn values and EM1-like Sr and Nd isotopic compositions, suggesting an important contribution from a metasomatized SCLM. The δ^{26}Mg and

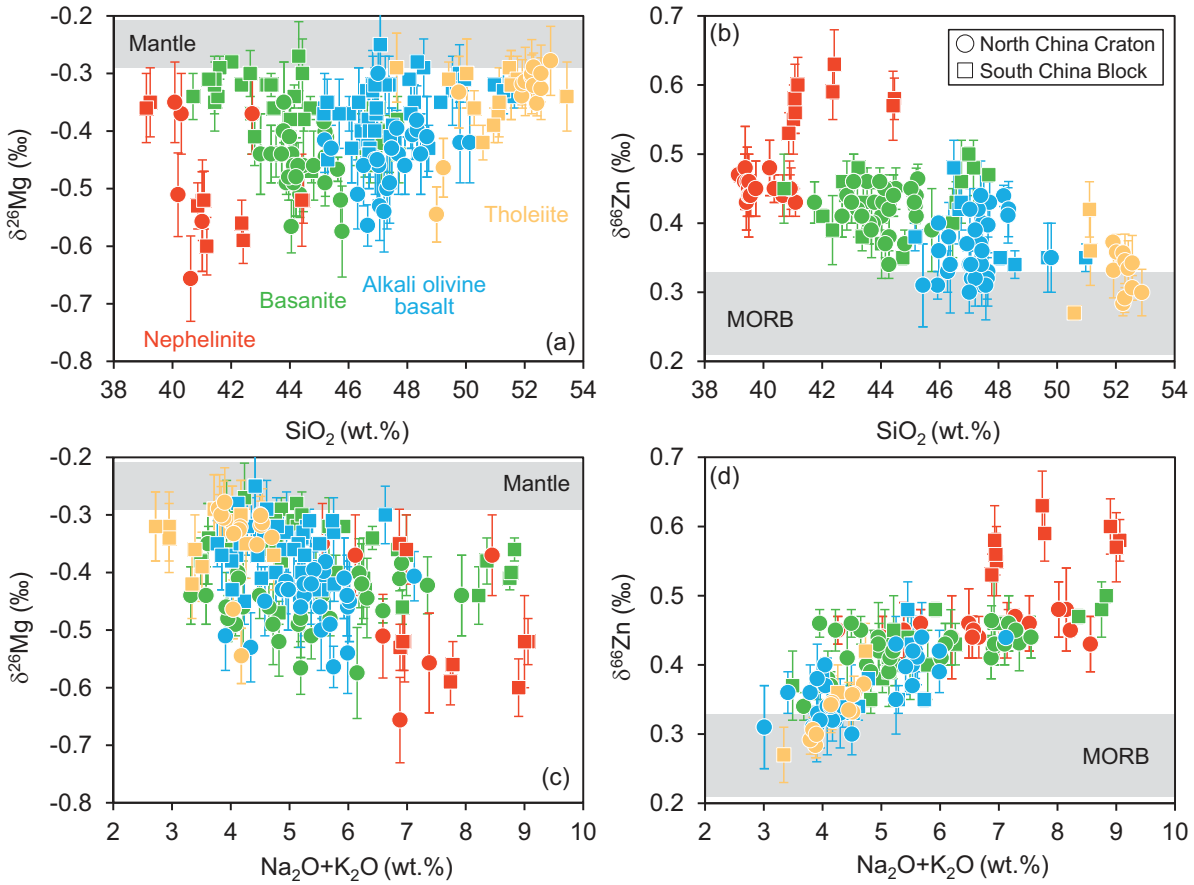

Fig. 15. Plots of (a) $\delta^{26}Mg$ vs SiO_2, (b) $\delta^{66}Zn$ vs SiO_2, (c) $\delta^{26}Mg$ vs Na_2O+K_2O, and (d) $\delta^{66}Zn$ vs Na_2O+K_2O for Cenozoic basalts from the North China Craton and South China Block. Compiled data are given in the Supplementary Data Table S2.

$\delta^{66}Zn$ values of alkaline and tholeiitic basalts are near-linearly correlated with each other and with alkalinity, incompatible trace element concentrations and Sr-Nd isotopic compositions. These correlations cannot be explained by varying degrees of partial melting of a single source at various pressures, but are consistent with interaction of carbonated silicate melts parental to alkaline basalts with partial melts from the metasomatized SCLM. We suggest partial melting of carbonated mantle and subsequent interaction of carbonated silicate melts with the SCLM to be a common process producing compositional diversity of intracontinental alkaline and tholeiitic basalts. Our study also indicates that infiltration of carbonated alkaline basaltic melts into the SCLM may reactivate the lithospheric keel and cause lithospheric thinning in ancient cratons such as the North China Craton.

ACKNOWLEDGMENTS

We are grateful to Meng-Lun Li, Hua-Ye Zhai, Chun Yang and Chun-Yang Liu for their assistance in the field and lab. Constructive comments from Dr. Sonja Aulbach and two anonymous reviewers significantly improve the quality of the manuscript and are highly appreciated. We also acknowledge Profs. Georg Zellmer and Gerhard Wörner for the careful and effective editorial handling.

FUNDING

This work is funded by the National Key Research and Development Project of China (2019YFA0708400), the National Natural Science Foundation of China (41730214), the 'Strategic Priority Research Program' of the Chinese Academy of Sciences (XDB18000000), and the National Key Research and Development Project of China (2016YFC0600310) to S.A.L.

SUPPLEMENTARY DATA

Supplementary data are available at *Journal of Petrology* online.

REFERENCES

Ague, J. J. & Nicolescu, S. (2014). Carbon dioxide released from subduction zones by fluid-mediated reactions. *Nature Geoscience* **7**, 355–360.

An, Y., Wu, F., Xiang, Y., Nan, X., Yu, X., Yang, J., Yu, H., Xie, L. & Huang, F. (2014). High-precision Mg isotope analyses of low-Mg rocks by MC-ICP-MS. *Chemical Geology* **390**, 9–21.

Aulbach, S. (2018). Cratonic lithosphere discontinuities: dynamics of small-volume melting, metacratonization, and a possible role for brines. In: Yuan H, Romanowicz B (eds) *Lithospheric Discontinuities geophysical monograph 239.* American Geophysical Union, Washington, D.C., pp. 177–204.

Aulbach, S., Lin, A. B., Weiss, Y. & Yaxley, G. M. (2020). Wehrlites from continental mantle monitor the passage and degassing of carbonated melts. *Geochemical Perspectives Letters* **15**, 30–34.

Aulbach, S., Sun, J., Tappe, S., Höfer, H. E. & Gerdes, A. (2017). Volatile-rich Metasomatism in the Cratonic Mantle beneath SW Greenland: link to Kimberlites and Mid-lithospheric Discontinuities. *Journal of Petrology* **58**, 2311–2338.

Basu, A. R., Junwen, W., Wankang, H., Guanghong, X. & Tatsumoto, M. (1991). Major element, REE, and Pb, Nd and Sr isotopic geochemistry of Cenozoic volcanic rocks of eastern China: implications for their origin from suboceanic-type mantle reservoirs. *Earth Planetary Science Letters* **105**, 149–169.

Bentahila, Y., Othman, D. B. & Luck, J.-M. (2008). Strontium, lead and zinc isotopes in marine cores as tracers of sedimentary provenance: A case study around Taiwan orogen. *Chemical Geology* **248**, 62–82.

Beunon, H., Mattielli, N., Doucet, L. S., Moine, B. & Debret, B. (2020). Mantle heterogeneity through Zn systematics in oceanic basalts: evidence for a deep carbon cycling. *Earth-Science Reviews* **205**, 103174.

Brewer, A. W., Teng, F.-Z. & Mullen, E. (2018). Magnesium isotopes as a tracer of crustal materials in volcanic arc magmas in the Northern Cascade Arc. *Frontiers in Earth Science* **6**, 21.

Brombin, V., Bonadiman, C., Coltorti, M., Fahnestock, M. F., Bryce, J. G. & Marzoli, A. (2018). Refertilized mantle keel below the Southern Alps domain (North-East Italy): evidence from Marosticano refractory mantle peridotites. *Lithos* **300–301**, 72–85.

Brombin, V., Bonadiman, C., Jourdan, F., Roghi, G., Coltorti, M., Webb, L. E., Callegaro, S., Bellieni, G., De Vecchi, G., Sedea, R. & Marzoli, A. (2019). Intraplate magmatism at a convergent plate boundary: the case of the Cenozoic northern Adria magmatism. *Earth-Science Reviews* **192**, 355–378.

Cai, R., Liu, J., Pearson, D. G., Li, D., Xu, Y., Liu, S.-A., Chu, Z., Chen, L.-H. & Li, S. (2021). Oxidation of the deep big mantle wedge by recycled carbonates: constraints from highly siderophile elements and osmium isotopes. *Geochimica et Cosmochimica Acta* **295**, 207–223.

Chen, C. Y., Frey, F. A., Garcia, M. O., Dalrymple, G. B. & Hart, S. R. (1991). The tholeiite to alkalic basalt transition at Haleakala Volcano, Maui, Hawaii. *Contributions to Mineralogy and Petrology* **106**, 183–200.

Chen, H., Savage, P. S., Teng, F.-Z., Helz, R. T. & Moynier, F. (2013). Zinc isotope fractionation during magmatic differentiation and the isotopic composition of the bulk Earth. *Earth and Planetary Science Letters* **369**, 34–42.

Chen, S., Liu, Y., Hu, J., Zhang, Z., Hou, Z., Huang, F. & Yu, H. (2015). Zinc isotopic compositions of NIST SRM 683 and whole-rock reference materials. *Geostandards and Geoanalytical Research* **40**, 417–432.

Dalton, J. A. & Wood, B. J. (1993). The compositions of primary carbonate melts and their evolution through wallrock reaction in the mantle. *Earth and Planetary Science Letters* **119**, 511–525.

Dasgupta, R., Hirschmann, M. M. & Smith, N. D. (2007). Partial melting experiments of peridotite+ CO2 at 3 GPa and genesis of alkalic ocean island basalts. *Journal of Petrology* **48**, 2093–2124.

Dasgupta, R., Mallik, A., Tsuno, K., Withers, A. C., Hirth, G. & Hirschmann, M. M. (2013). Carbon-dioxide-rich silicate melt in the Earth's upper mantle. *Nature* **493**, 211–215.

Debret, B., Beunon, H., Mattielli, N., Andreani, M., Da Costa, I. R. & Escartin, J. (2018a). Ore component mobility, transport and mineralization at mid-oceanic ridges: a stable isotopes (Zn, Cu and Fe) study of the Rainbow massif (Mid-Atlantic Ridge 36° 14′ N). *Earth and Planetary Science Letters* **503**, 170–180.

Debret, B., Bouilhol, P., Pons, M. L. & Williams, H. (2018b). Carbonate transfer during the onset of slab devolatilization: new insights from Fe and Zn stable isotopes. *Journal of Petrology* **59**, 1145–1166.

Deng, L., Liu, Y., Zong, K., Zhu, L., Xu, R., Hu, Z. & Gao, S. (2017). Trace element and S r isotope records of multi-episode carbonatite metasomatism on the eastern margin of the N orth C hina C raton. *Geochemistry, Geophysics, Geosystems* **18**, 220–237.

Doucet, L. S., Mattielli, N., Ionov, D. A., Debouge, W. & Golovin, A. V. (2016). Zn isotopic heterogeneity in the mantle: a melting control? *Earth and Planetary Science Letters* **451**, 232–240.

Ducher, M., Blanchard, M. & Balan, E. (2016). Equilibrium zinc isotope fractionation in Zn-bearing minerals from first-principles calculations. *Chemical Geology* **443**, 87–96.

Fan, Q. & Hooper, P. R. (1991). The Cenozoic basaltic rocks of eastern China: petrology and chemical composition. *Journal of Petrology* **32**, 765–810.

Fan, W., Zhang, H., Baker, J., Jarvis, K., Mason, P. & Menzies, M. (2000). On and off the North China Craton: where is the Archaean keel? *Journal of Petrology* **41**, 933–950.

Frezzotti, M. L., Selverstone, J., Sharp, Z. D. & Compagnoni, R. (2011). Carbonate dissolution during subduction revealed by diamond-bearing rocks from the Alps. *Nature Geoscience* **4**, 703–706.

Fukao, Y., Obayashi, M., Nakakuki, T. & the Deep Slab Project Group (2009). Stagnant slab: a review. *Annual Review of Earth and Planetary Sciences* **37**, 19–46.

Gao, T., Ke, S., Li, R., Meng, X. N., He, Y., Liu, C., Wang, Y., Li, Z. & Zhu, J. M. (2019). High-precision magnesium isotope analysis of geological and environmental reference materials by multiple-collector inductively coupled plasma mass spectrometry. *Rapid Communications in Mass Spectrometry : Rcm* **33**, 767–777.

Geng, X., Foley, S. F., Liu, Y., Wang, Z., Hu, Z. & Zhou, L. (2019). Thermal-chemical conditions of the North China Mesozoic lithospheric mantle and implication for the lithospheric thinning of cratons. *Earth and Planetary Science Letters* **516**, 1–11.

Gerbode, C. & Dasgupta, R. (2010). Carbonate-fluxed melting of MORB-like pyroxenite at 2·9 GPa and genesis of HIMU ocean island basalts. *Journal of Petrology* **51**, 2067–2088.

Guo, P., Niu, Y., Sun, P., Gong, H. & Wang, X. (2020). Lithosphere thickness controls continental basalt compositions: An illustration using Cenozoic basalts from eastern China. *Geology* **48**, 128–133.

Hart, S. R., Hauri, E. H., Oschmann, L. A. & Whitehead, J. A. (1992). Mantle plumes and entrainment: isotopic evidence. *Science (New York, N.Y.)* **256**, 517–520.

He, Y., Meng, X., Ke, S., Wu, H., Zhu, C., Teng, F.-Z., Hoefs, J., Huang, J., Yang, W., Xu, L., Hou, Z., Ren, Z.-Y. & Li, S. (2019). A nephelinitic component with unusual δ^{56}Fe in Cenozoic basalts from eastern China and its implications for deep oxygen cycle. *Earth and Planetary Science Letters* **512**, 175–183.

Hirose, K. (1997). Partial melt compositions of carbonated peridotite at 3 GPa and role of CO2 in alkali-basalt magma generation. *Geophysical Research Letters* **24**, 2837–2840.

Hirschmann, M. M., Kogiso, T., Baker, M. B. & Stolper, E. M. (2003). Alkalic magmas generated by partial melting of garnet pyroxenite. *Geology* **31**, 481–484.

Hofmann, A. W. (2014). Sampling Mantle Heterogeneity through Oceanic Basalts: isotopes and Trace Elements. In: Holland, H. D. & Turekian, K. K. (eds) *Treatise on Geochemistry*, 2nd edn. Oxford: Elsevier, pp. 67–101.

Hong, L., Xu, Y., Zhang, L., Liu, Z., Xia, X. & Kuang, Y. (2020b). Oxidized Late Mesozoic subcontinental lithospheric mantle beneath the eastern North China Craton: a clue to understanding cratonic destruction. *Gondwana Research* **81**, 230–239.

Hong, L., Xu, Y.-G., Zhang, L., Wang, Y. & Ma, L. (2020a). Recycled carbonate-induced oxidization of the convective mantle beneath Jiaodong, Eastern China. *Lithos* **366-367**, 105544.

Hu, Y., Teng, F.-Z. & Ionov, D. A. (2020). Magnesium isotopic composition of metasomatized upper sub-arc mantle and its implications to Mg cycling in subduction zones. *Geochimica et Cosmochimica Acta* **278**, 219–234.

Hu, Y., Teng, F.-Z., Plank, T. & Huang, K.-J. (2017). Magnesium isotopic composition of subducting marine sediments. *Chemical Geology* **466**, 15–31.

Huang, J., Ackerman, L., Zhang, X. C. & Huang, F. (2019). Mantle Zn isotopic heterogeneity caused by melt-rock reaction: evidence from Fe-rich peridotites and pyroxenites from the Bohemian Massif, Central Europe. *Journal of Geophysical Research: Solid Earth* **124**, 3588–3604.

Huang, J., Chen, S., Zhang, X. C. & Huang, F. (2018a). Effects of melt percolation on Zn isotope heterogeneity in the mantle: constraints from peridotite massifs in Ivrea-Verbano Zone, Italian Alps. *Journal of Geophysical Research: Solid Earth* **123**, 2706–2722.

Huang, J., Ke, S., Gao, Y., Xiao, Y. & Li, S. (2015a). Magnesium isotopic compositions of altered oceanic basalts and gabbros from IODP Site 1256 at the East Pacific Rise. *Lithos* **231**, 53–61.

Huang, J., Li, S.-G., Xiao, Y., Ke, S., Li, W.-Y. & Tian, Y. (2015b). Origin of low δ^{26}Mg Cenozoic basalts from South China Block and their geodynamic implications. *Geochimica et Cosmochimica Acta* **164**, 298–317.

Huang, J., Liu, S. A., Gao, Y., Xiao, Y. & Chen, S. (2016). Copper and zinc isotope systematics of altered oceanic crust at IODP Site 1256 in the eastern equatorial Pacific. *Journal of Geophysical Research: Solid Earth* **121**, 7086–7100.

Huang, J., Zhang, X.-C., Chen, S., Tang, L., Wörner, G., Yu, H. & Huang, F. (2018b). Zinc isotopic systematics of Kamchatka-Aleutian arc magmas controlled by mantle melting. *Geochimica et Cosmochimica Acta* **238**, 85–101.

Huang, J. & Zhao, D. (2006). High-resolution mantle tomography of China and surrounding regions. *Journal of Geophysical Research* **111**, B09305

Huang, K.-J., Teng, F.-Z., Elsenouy, A., Li, W.-Y. & Bao, Z.-Y. (2013). Magnesium isotopic variations in loess: Origins and implications. *Earth and Planetary Science Letters* **374**, 60–70.

Huang, K.-J., Teng, F.-Z., Plank, T., Staudigel, H., Hu, Y. & Bao, Z.-Y. (2018c). Magnesium isotopic composition of altered oceanic crust and the global Mg cycle. *Geochimica et Cosmochimica Acta* **238**, 357–373.

Inglis, E. C., Debret, B., Burton, K. W., Millet, M.-A., Pons, M.-L., Dale, C. W., Bouilhol, P., Cooper, M., Nowell, G. M., McCoy-West, A. J. & Williams, H. M. (2017). The behaviour of iron and zinc stable isotopes accompanying the subduction of mafic oceanic crust: A case study from Western Alpine Ophiolites. *Geochemistry, Geophysics, Geosystems* **18**, 2562–2579.

Ionov, D. A., Chanefo, I. & Bodinier, J.-L. (2005). Origin of Fe-rich lherzolites and wehrlites from Tok, SE Siberia by reactive melt percolation in refractory mantle peridotites. *Contributions to Mineralogy and Petrology* **150**, 335–353.

Jin, Q.-Z., Huang, J., Liu, S.-C. & Huang, F. (2020). Magnesium and zinc isotope evidence for recycled sediments and oceanic crust in the mantle sources of continental basalts from eastern China. *Lithos* **370-371**, 105627.

Ke, S., Teng, F.-Z., Li, S.-G., Gao, T., Liu, S.-A., He, Y. & Mo, X. (2016). Mg, Sr, and O isotope geochemistry of syenites from northwest Xinjiang, China: Tracing carbonate recycling during Tethyan oceanic subduction. *Chemical Geology* **437**, 109–119.

Kelemen, P. B. & Manning, C. E. (2015). Reevaluating carbon fluxes in subduction zones, what goes down, mostly comes up. *Proceedings of the National Academy of Sciences* **112** (**30**), E3997–E4006.

Kerrick, D. & Connolly, J. (2001). Metamorphic devolatilization of subducted marine sediments and the transport of volatiles into the Earth's mantle. *Nature* **411**, 293–296.

Keshav, S., Gudfinnsson, G. H., Sen, G. & Fei, Y. (2004). High-pressure melting experiments on garnet clinopyroxenite and the alkalic to tholeiitic transition in ocean-island basalts. *Earth and Planetary Science Letters* **223**, 365–379.

Kogiso, T. & Hirschmann, M. M. (2006). Partial melting experiments of bimineralic eclogite and the role of recycled mafic oceanic crust in the genesis of ocean island basalts. *Earth and Planetary Science Letters* **249**, 188–199.

Kogiso, T., Hirschmann, M. M. & Frost, D. J. (2003). High-pressure partial melting of garnet pyroxenite: possible mafic lithologies in the source of ocean island basalts. *Earth and Planetary Science Letters* **216**, 603–617.

Kunzmann, M., Halverson, G. P., Sossi, P. A., Raub, T. D., Payne, J. L. & Kirby, J. (2013). Zn isotope evidence for immediate resumption of primary productivity after snowball Earth. *Geology* **41**, 27–30.

Lambart, S., Laporte, D., Provost, A. & Schiano, P. (2012). Fate of pyroxenite-derived melts in the peridotitic mantle: thermodynamic and experimental constraints. *Journal of Petrology* **53**, 451–476.

Lassiter, J. C. & DePaolo, D. J. (1997). Plume/lithosphere interaction in the generation of continental and oceanic flood basalts: chemical and isotopic constraints. In: Mahoney J & Coffin B (eds) Large Igneous Provinces: Continental, Oceanic and Planetary Flood Volcanism, AGU Geophysical Monograph , vol. 100, AGU, Washington, D.C., pp. 335–356.

Le Bas, M. J. L., Le Maitre, R. W., Streckeisen, A., Zanettin, B. & IUGS Subcommission on the Systematics of Igneous Rocks (1986). A chemical classification of volcanic rocks based on the total alkali-silica diagram. *Journal of Petrology* **27**, 745–750.

Li, S.-G. & Wang, Y. (2018). Formation time of the big mantle wedge beneath eastern China and a new lithospheric thinning mechanism of the North China craton—Geodynamic effects of deep recycled carbon. Science China Earth Sciences **61**, 853–868.

Li, J.-L., Klemd, R., Gao, J. & Meyer, M. (2014a). Compositional zoning in dolomite from lawsonite-bearing eclogite (SW Tianshan, China): Evidence for prograde metamorphism during subduction of oceanic crust. *American Mineralogist* **99**, 206–217.

Li, M.-L., Liu, S.-A., Lee, H.-Y., Yang, C. & Wang, Z.-Z. (2021). Magnesium and zinc isotopic anomaly of Cenozoic lavas in central Myanmar: Origins and implications for deep carbon recycling. *Lithos* **386-387**, 106011.

Li, S.-G., Yang, W., Ke, S., Meng, X., Tian, H., Xu, L., He, Y., Huang, J., Wang, X.-C., Xia, Q., Sun, W., Yang, X., Ren, Z.-Y., Wei, H., Liu, Y., Meng, F. & Yan, J. (2017). Deep carbon cycles constrained by a large-scale mantle Mg isotope anomaly in eastern China. *National Science Review* **4**, 111–120.

Li, W.-Y., Teng, F.-Z., Ke, S., Rudnick, R. L., Gao, S., Wu, F.-Y. & Chappell, B. (2010). Heterogeneous magnesium isotopic composition of the upper continental crust. *Geochimica et Cosmochimica Acta* **74**, 6867–6884.

Li, W. Y., Teng, F. Z., Wing, B. A. & Xiao, Y. (2014b). Limited magnesium isotope fractionation during metamorphic dehydration in metapelites from the Onawa contact aureole. *Geochemistry, Geophysics, Geosystems* **15**, 408–415.

Lin, A. B., Zheng, J. P., Aulbach, S., Xiong, Q., Pan, S. K. & Gerdes, A. (2020). Causes and Consequences of Wehrlitization Beneath a Trans-Lithospheric Fault: Evidence From Mesozoic Basalt-Borne Wehrlite Xenoliths From the Tan-Lu Fault Belt, North China Craton. *Journal of Geophysical Research: Solid Earth* **125**, e2019JB019084.

Little, S. H., Vance, D., McManus, J. & Severmann, S. (2016). Key role of continental margin sediments in the oceanic mass balance of Zn and Zn isotopes. *Geology* **44**, 207–210.

Liu, J., Carlson, R. W., Rudnick, R. L., Walker, R. J., Gao, S. & Wu, F-y. (2012). Comparative Sr–Nd–Hf–Os–Pb isotope systematics of xenolithic peridotites from Yangyuan, North China Craton: additional evidence for a Paleoproterozoic age. *Chemical Geology* **332–333**, 1–14.

Liu, P.-P., Teng, F.-Z., Dick, H. J. B., Zhou, M.-F. & Chung, S.-L. (2017a). Magnesium isotopic composition of the oceanic mantle and oceanic Mg cycling. *Geochimica et Cosmochimica Acta* **206**, 151–165.

Liu, S.-A., Li, D., Li, S., Teng, F.-Z., Ke, S., He, Y. & Lu, Y. (2014). High-precision copper and iron isotope analysis of igneous rock standards by MC-ICP-MS. *Journal of Analytical Atomic Spectrometry* **29**, 122–133.

Liu, S.-A. & Li, S.-G. (2019). Tracing the deep carbon cycle using metal stable isotopes: opportunities and challenges. *Engineering* **5**, 448–457.

Liu, S.-A., Liu, P.-P., Lv, Y., Wang, Z.-Z. & Dai, J.-G. (2019). Cu and Zn isotope fractionation during oceanic alteration: implications for oceanic Cu and Zn cycles. *Geochimica et Cosmochimica Acta* **257**, 191–205.

Liu, S.-A., Wang, Z.-Z., Li, S.-G., Huang, J. & Yang, W. (2016). Zinc isotope evidence for a large-scale carbonated mantle beneath eastern China. *Earth and Planetary Science Letters* **444**, 169–178.

Liu, S.-A., Wang, Z. Z., Yang, C., Li, S. G. & Ke, S. (2020). Mg and Zn isotope evidence for two types of mantle metasomatism and deep recycling of magnesium carbonates. *Journal of Geophysical Research: Solid Earth* **125**, e2020JB020684.

Liu, S.-A., Wu, H., Shen, S-Z., Jiang, G., Zhang, S., Lv, Y., Zhang, H. & Li, S. (2017b). Zinc isotope evidence for intensive magmatism immediately before the end-Permian mass extinction. *Geology* **45**, 343–346.

Liu, X., Zhao, D., Li, S. & Wei, W. (2017c). Age of the subducting Pacific slab beneath East Asia and its geodynamic implications. *Earth and Planetary Science Letters* **464**, 166–174.

Liu, Y., Gao, S., Kelemen, P. B. & Xu, W. (2008). Recycled crust controls contrasting source compositions of Mesozoic and Cenozoic basalts in the North China Craton. *Geochimica et Cosmochimica Acta* **72**, 2349–2376.

Lundstrom, C. C. (2000). Rapid diffusive infiltration of sodium into partially molten peridotite. *Nature* **403**, 527–530.

Lustrino, M., Melluso, L. & Morra, V. (2002). The transition from alkaline to tholeiitic magmas: a case study from the Orosei-Dorgali Pliocene volcanic district (NE Sardinia, Italy). *Lithos* **63**, 83–113.

Lustrino, M. & Wilson, M. (2007). The circum-Mediterranean anorogenic Cenozoic igneous province. *Earth-Science Reviews* **81**, 1–65.

Lv, Y., Liu, S.-A., Wu, H., Hohl, S. V., Chen, S. & Li, S. (2018). Zn-Sr isotope records of the Ediacaran Doushantuo Formation in South China: diagenesis assessment and implications. *Geochimica et Cosmochimica Acta* **239**, 330–345.

Ma, L., Teng, F.-Z., Jin, L., Ke, S., Yang, W., Gu, H.-O. & Brantley, S. L. (2015). Magnesium isotope fractionation during shale weathering in the Shale Hills Critical Zone Observatory: Accumulation of light Mg isotopes in soils by clay mineral transformation. *Chemical Geology* **397**, 37–50.

Macris, C. A., Young, E. D. & Manning, C. E. (2013). Experimental determination of equilibrium magnesium isotope fractionation between spinel, forsterite, and magnesite from 600 to 800 C. *Geochimica et. Geochimica et Cosmochimica Acta* **118**, 18–32.

Mallik, A. & Dasgupta, R. (2014). Effect of variable CO_2 on eclogite-derived andesite and lherzolite reaction at 3 GPa—Implications for mantle source characteristics of alkalic ocean island basalts. *Geochemistry, Geophysics, Geosystems* **15**, 1533–1557.

Malusà, M. G., Frezzotti, M. L., Ferrando, S., Brandmayr, E., Romanelli, F. & Panza, G. F. (2018). Active carbon sequestration in the Alpine mantle wedge and implications for long--term climate trends. *Scientific Reports* **8**, 1–8.

Maréchal, C., Telouk, P. & Albarede, F. (1999). Precise analysis of copper and zinc isotopic compositions by plasma-source mass spectrometry. *Chemical Geology* **156**, 251–273.

McCoy-West, A. J., Fitton, J. G., Pons, M.-L., Inglis, E. C. & Williams, H. M. (2018). The Fe and Zn isotope composition of deep mantle source regions: Insights from Baffin Island picrites. *Geochimica et Cosmochimica Acta* **238**, 542–562.

McDonough, W. F. & Sun, S.-S. (1995). The composition of the Earth. *Chemical Geology* **120**, 223–253.

Melluso, L., Cucciniello, C., le Roex, A. P. & Morra, V. (2016). The geochemistry of primitive volcanic rocks of the Ankaratra volcanic complex, and source enrichment processes in the genesis of the Cenozoic magmatism in Madagascar. *Geochimica et Cosmochimica Acta* **185**, 435–452.

Merlini, M., Crichton, W. A., Hanfland, M., Gemmi, M., Müller, H., Kupenko, I. & Dubrovinsky, L. (2012). Structures of dolomite at ultrahigh pressure and their influence on the deep carbon cycle. *Proceedings of the National Academy of Sciences* **109**, 13509–13514.

Pan, D., Spanu, L., Harrison, B., Sverjensky, D. A. & Galli, G. (2013). Dielectric properties of water under extreme conditions and transport of carbonates in the deep Earth. *Proceedings of the National Academy of Sciences* **110**, 6646–6650.

Pang, K.-N., Teng, F.-Z., Sun, Y., Chung, S.-L. & Zarrinkoub, M. H. (2020). Magnesium isotopic systematics of the Makran arc magmas, Iran: Implications for crust-mantle Mg isotopic balance. *Geochimica et Cosmochimica Acta* **278**, 110–121.

Pichat, S., Douchet, C. & Albarède, F. (2003). Zinc isotope variations in deep-sea carbonates from the eastern equatorial Pacific over the last 175 ka. *Earth and Planetary Science Letters* **210**, 167–178.

Pilet, S., Baker, M. B. & Stolper, E. M. (2008). Metasomatized lithosphere and the origin of alkaline lavas. *Science (New York, N.Y.)* **320**, 916–919.

Plank, T. & Manning, C. E. (2019). Subducting carbon. *Nature* **574**, 343–352.

Poli, S. (2015). Carbon mobilized at shallow depths in subduction zones by carbonatitic liquids. *Nature Geoscience* **8**, 633–636.

Pons, M.-L., Debret, B., Bouilhol, P., Delacour, A. & Williams, H. (2016). Zinc isotope evidence for sulfate-rich fluid transfer across subduction zones. *Nature Communications* **7**, 13794.

Pons, M.-L., Quitté, G., Fujii, T., Rosing, M. T., Reynard, B., Moynier, F., Douchet, C. & Albarède, F. (2011). Early Archean serpentine mud volcanoes at Isua, Greenland, as a niche for early life. *Proceedings of the National Academy of Sciences* **108**, 17639–17643.

Regier, M. E., Pearson, D. G., Stachel, T., Luth, R. W., Stern, R. A. & Harris, J. W. (2020). The lithospheric-to-lower-mantle carbon cycle recorded in superdeep diamonds. *Nature* **585**, 234–238.

Rudnick, R. L., Gao, S., Ling, W-L., Liu, Y-S. & McDonough, W. F. (2004). Petrology and geochemistry of spinel peridotite xenoliths from Hannuoba and Qixia, North China craton. *Lithos* **77**, 609–637.

Russell, J. K., Porritt, L. A., Lavallée, Y. & Dingwell, D. B. J. N. (2012). Kimberlite ascent by assimilation-fuelled buoyancy. *Nature* **481**, 352–356.

Sakuyama, T., Tian, W., Kimura, J.-I., Fukao, Y., Hirahara, Y., Takahashi, T., Senda, R., Chang, Q., Miyazaki, T., Obayashi, M., Kawabata, H. & Tatsumi, Y. (2013). Melting of dehydrated oceanic crust from the stagnant slab and of the hydrated mantle transition zone: Constraints from Cenozoic alkaline basalts in eastern China. *Chemical Geology* **359**, 32–48.

Sato, K. & Katsura, T. (2001). Experimental investigation on dolomite dissociation into aragonite+ magnesite up to 8.5 GPa. *Earth and Planetary Science Letters* **184**, 529–534.

Scott, J. M., Hodgkinson, A., Palin, J. M., Waight, T. E., Van der Meer, Q. H. A. & Cooper, A. F. (2014). Ancient melt depletion overprinted by young carbonatitic metasomatism in the New Zealand lithospheric mantle. *Contributions to Mineralogy and Petrology* **167**, 963.

Sobolev, A. V., Hofmann, A. W., Kuzmin, D. V., Yaxley, G. M., Arndt, N. T., Chung, S.-L., Danyushevsky, L. V., Elliott, T., Frey, F. A., Garcia, M. O., Gurenko, A. A., Kamenetsky, V. S., Kerr, A. C., Krivolutskaya, N. A., Matvienkov, V. V., Nikogosian, I. K., Rocholl, A., Sigurdsson, I. A., Sushchevskaya, N. M. & Teklay, M. (2007). The amount of recycled crust in sources of mantle-derived melts. *Science (New York, N.Y.)* **316**, 412–417.

Song, Y. & Frey, F. A. (1989). Geochemistry of peridotite xenoliths in basalt from Hannuoba, eastern China: implications for subcontinental mantle heterogeneity. *Geochimica et Cosmochimica Acta* **53**, 97–113.

Song, Y., Frey, F. A. & Zhi, X. (1990). Isotopic characteristics of Hannuoba basalts, eastern China: implications for their petrogenesis and the composition of subcontinental mantle. *Chemical Geology* **88**, 35–52.

Sossi, P. A., Halverson, G. P., Nebel, O. & Eggins, S. M. (2015). Combined separation of Cu, Fe and Zn from rock matrices and improved analytical protocols for stable isotope determination. *Geostandards and Geoanalytical Research* **39**, 129–149.

Sossi, P. A., Nebel, O., O'Neill, H. S. C. & Moynier, F. (2018). Zinc isotope composition of the Earth and its behaviour during planetary accretion. *Chemical Geology* **477**, 73–84.

Stracke, A., Hofmann, A. W. & Hart, S. R. (2005). FOZO, HIMU, and the rest of the mantle zoo. *Geochemistry, Geophysics, Geosystems* **6**, Q05007 10.1029/2004GC000824.

Stracke, A., Tipper, E. T., Klemme, S. & Bizimis, M. (2018). Mg isotope systematics during magmatic processes: Inter-mineral fractionation in mafic to ultramafic Hawaiian xenoliths. *Geochimica et Cosmochimica Acta* **226**, 192–205.

Su, B.-X., Hu, Y., Teng, F.-Z., Xiao, Y., Zhang, H.-F., Sun, Y., Bai, Y., Zhu, B., Zhou, X.-H. & Ying, J.-F. (2019). Light Mg isotopes in mantle-derived lavas caused by chromite crystallization, instead of carbonatite metasomatism. *Earth and Planetary Science Letters* **522**, 79–86.

Su, B.-X., Hu, Y., Teng, F.-Z., Xiao, Y., Zhou, X.-H., Sun, Y., Zhou, M.-F. & Chang, S.-C. (2017). Magnesium isotope constraints on subduction contribution to Mesozoic and Cenozoic East Asian continental basalts. *Chemical Geology* **466**, 116–122.

Sun, C., Liu, J., Xu, B. & You, H. (2019). First radiocarbon dating of a Holocene eruption of the Datong volcanic field, eastern China. *Journal of Volcanology and Geothermal Research* **384**, 275–279.

Sweere, T. C., Dickson, A. J., Jenkyns, H. C., Porcelli, D., Elrick, M., van den Boorn, S. H. J. M. & Henderson, G. M. (2018). Isotopic evidence for changes in the zinc cycle during Oceanic Anoxic Event 2 (Late Cretaceous). *Geology* **46**, 463–466.

Tang, Y.-J., Zhang, H.-F., Nakamura, E. & Ying, J.-F. (2011). Multistage melt/fluid-peridotite interactions in the refertilized lithospheric mantle beneath the North China Craton: constraints from the Li–Sr–Nd isotopic disequilibrium between minerals of peridotite xenoliths. *Contributions to Mineralogy and Petrology* **161**, 845–861.

Tang, Y.-J., Zhang, H.-F. & Ying, J.-F. (2006). Asthenosphere–lithospheric mantle interaction in an extensional regime: implication from the geochemistry of Cenozoic basalts from Taihang Mountains, North China Craton. *Chemical Geology* **233**, 309–327.

Tang, Y.-J., Zhang, H.-F., Ying, J.-F., Su, B.-X., Chu, Z.-Y., Xiao, Y. & Zhao, X.-M. (2013). Highly heterogeneous lithospheric mantle beneath the Central Zone of the North China Craton evolved from Archean mantle through diverse melt refertilization. *Gondwana Research* **23**, 130–140.

Tang, Y.-J., Zhang, H.-F., Ying, J.-F., Zhang, J. & Liu, X.-M. (2008). Refertilization of ancient lithospheric mantle beneath the central North China Craton: evidence from petrology and geochemistry of peridotite xenoliths. *Lithos* **101**, 435–452.

Teng, F.-Z. (2017). Magnesium isotope geochemistry. *Reviews in Mineralogy and Geochemistry* **82**, 219–287.

Teng, F.-Z., Hu, Y. & Chauvel, C. (2016). Magnesium isotope geochemistry in arc volcanism. *Proceedings of the National Academy of Sciences* **113**, 7082–7087.

Teng, F.-Z., Li, W.-Y., Ke, S., Marty, B., Dauphas, N., Huang, S., Wu, F.-Y. & Pourmand, A. (2010). Magnesium isotopic composition of the Earth and chondrites. *Geochimica et Cosmochimica Acta* **74**, 4150–4166.

Teng, F.-Z., Wadhwa, M. & Helz, R. T. (2007). Investigation of magnesium isotope fractionation during basalt differentiation: implications for a chondritic composition of the terrestrial mantle. *Earth and Planetary Science Letters* **261**, 84–92.

Teng, F. Z., Li, W. Y., Ke, S., Yang, W., Liu, S. A., Sedaghatpour, F., Wang, S. J., Huang, K. J., Hu, Y. & Ling, M. X. (2015). Magnesium isotopic compositions of international geological reference materials. *Geostandards and Geoanalytical Research* **3**, 329–339.

Thirlwall, M. F. (1997). Pb isotopic and elemental evidence for OIB derivation from young HIMU mantle. *Chemical Geology* **139**, 51–74.

Thomson, A. R., Walter, M. J., Kohn, S. C. & Brooker, R. A. (2016). Slab melting as a barrier to deep carbon subduction. *Nature* **529**, 76–79.

Tian, H., Yang, W., Li, S.-G., Ke, S. & Chu, Z. (2016). Origin of low δ^{26}Mg basalts with EM-I component: Evidence for

interaction between enriched lithosphere and carbonated asthenosphere. *Geochimica et Cosmochimica Acta* **188**, 93–105.

Timm, C., Hoernle, K., Werner, R., Hauff, F., van den Bogaard, P., White, J., Mortimer, N. & Garbe-Schönberg, D. (2010). Temporal and geochemical evolution of the Cenozoic intraplate volcanism of Zealandia. *Earth-Science Reviews* **98**, 38–64.

Walter, M. J. (1998). Melting of garnet peridotite and the origin of komatiite and depleted lithosphere. *Journal of Petrology* **39**, 29–60.

Wang, S.-J., Teng, F.-Z., Li, S.-G. & Hong, J.-A. (2014). Magnesium isotopic systematics of mafic rocks during continental subduction. *Geochimica et Cosmochimica Acta* **143**, 34–48.

Wang, S.-J., Teng, F.-Z., Rudnick, R. L. & Li, S.-G. (2015). The behavior of magnesium isotopes in low-grade metamorphosed mudrocks. *Geochimica et Cosmochimica Acta* **165**, 435–448.

Wang, S.-J., Teng, F.-Z. & Scott, J. M. (2016). Tracing the origin of continental HIMU-like intraplate volcanism using magnesium isotope systematics. *Geochimica et Cosmochimica Acta* **185**, 78–87.

Wang, X., Liu, S.-A., Wang, Z., Chen, D. & Zhang, L. (2018a). Zinc and strontium isotope evidence for climate cooling and constraints on the Frasnian-Famennian (~372 Ma) mass extinction. *Palaeogeography, Palaeoclimatology, Palaeoecol ogy* **498**, 68–82.

Wang, X.-J., Chen, L.-H., Hofmann, A. W., Mao, F.-G., Liu, J.-Q., Zhong, Y., Xie, L.-W. & Yang, Y.-H. (2017a). Mantle transition zone-derived EM1 component beneath NE China: Geochemical evidence from Cenozoic potassic basalts. *Earth and Planetary Science Letters* **465**, 16–28.

Wang, Z.-Z., Liu, S.-A., Chen, L.-H., Li, S.-G. & Zeng, G. (2018b). Compositional transition in natural alkaline lavas through silica-undersaturated melt–lithosphere interaction. *Geology* **46**, 771–774.

Wang, Z.-Z., Liu, S.-A., Liu, J., Huang, J., Xiao, Y., Chu, Z.-Y., Zhao, X.-M. & Tang, L. (2017b). Zinc isotope fractionation during mantle melting and constraints on the Zn isotope composition of Earth's upper mantle. *Geochimica et Cosmochimica Acta* **198**, 151–167.

Wasylenki, L. E., Baker, M. B., Kent, A. J. & Stolper, E. M. (2003). Near-solidus melting of the shallow upper mantle: partial melting experiments on depleted peridotite. *Journal of Petrology* **44**, 1163–1191.

Willbold, M. & Stracke, A. (2006). Trace element composition of mantle end-members: Implications for recycling of oceanic and upper and lower continental crust. *Geochemistry, Geophysics, Geosystems* **7**, n/a–n/a.

Wilson, M., Downes, H. & Cebria, J.-M. (1995). Contrasting fractionation trends in coexisting continental alkaline magma series; Cantal, Massif Central, France. *Journal of Petrology* **36**, 1729–1753.

Wimpenny, J., Yin, Q.-Z., Tollstrup, D., Xie, L.-W. & Sun, J. (2014). Using Mg isotope ratios to trace Cenozoic weathering changes: a case study from the Chinese Loess Plateau. *Chemical Geology* **376**, 31–43.

Workman, R. K. & Hart, S. R. (2005). Major and trace element composition of the depleted MORB mantle (DMM). *Earth and Planetary Science Letters* **231**, 53–72.

Xiao, Y., Teng, F.-Z., Zhang, H.-F. & Yang, W. (2013). Large magnesium isotope fractionation in peridotite xenoliths from eastern North China craton: Product of melt–rock interaction. *Geochimica et Cosmochimica Acta* **115**, 241–261.

Xiao, Y., Zhang, H.-F., Fan, W.-M., Ying, J.-F., Zhang, J., Zhao, X.-M. & Su, B.-X. (2010). Evolution of lithospheric mantle beneath the Tan-Lu fault zone, eastern North China Craton: evidence from petrology and geochemistry of peridotite xenoliths. *Lithos* **117**, 229–246.

Xu, R., Liu, Y., Wang, X.-C., Foley, S. F., Zhang, Y. & Yuan, H. (2020). Generation of continental intraplate alkali basalts and implications for deep carbon cycle in the mantle transition zone. *Earth-Science Reviews* **201**, https://doi.org/10.1016/j.earscirev.2019.103073.

Xu, Y.-G., Blusztajn, J., Ma, J.-L., Suzuki, K., Liu, J.-F. & Hart, S. R. (2008). Late Archean to Early Proterozoic lithospheric mantle beneath the western North China craton: Sr–Nd–Os isotopes of peridotite xenoliths from Yangyuan and Fansi. *Lithos* **102**, 25–42.

Xu, Y.-G. & Bodinier, J.-L. (2004). Contrasting enrichments in high-and low-temperature mantle xenoliths from Nushan, Eastern China: results of a single metasomatic event during lithospheric accretion? *Journal of Petrology* **45**, 321–341.

Xu, Y.-G., Li, H.-Y., Hong, L.-B., Ma, L., Ma, Q. & Sun, M.-D. (2018). Generation of Cenozoic intraplate basalts in the big mantle wedge under eastern Asia. *Science China Earth Sciences* **61**, 869–886.

Xu, Y.-G., Ma, J.-L., Frey, F. A., Feigenson, M. D. & Liu, J.-F. (2005). Role of lithosphere–asthenosphere interaction in the genesis of Quaternary alkali and tholeiitic basalts from Datong, western North China Craton. *Chemical Geology* **224**, 247–271.

Xu, Y.-G., Mercier, J.-C C., Lin, C.-Y., Shi, L.-B., Menzies, M. A., Ross, J. V. & Harte, B. (1996). K-rich glass-bearing wehrlite xenoliths from Yitong, Northeastern China: petrological and chemical evidence for mantle metasomatism. *Contributions to Mineralogy and Petrology* **125**, 406–420.

Yamamoto, Y., Tsunakawa, H., Shaw, J. & Kono, M. (2007). Paleomagnetism of the Datong monogenetic volcanoes in China: paleodirection and paleointensity during the middle to early Brunhes Chron. *Earth, Planets and Space* **59**, 727–746.

Yang, C. & Liu, S. A. (2019). Zinc isotope constraints on recycled oceanic crust in the mantle sources of the Emeishan large igneous province. *Journal of Geophysical Research: Solid Earth* **124**, 12537–12555.

Yang, W. & Li, S. G. (2008). Geochronology and geochemistry of the Mesozoic volcanic rocks in Western Liaoning: Implications for lithospheric thinning of the North China Craton. *Lithos* **102**, 88–117.

Yang, W., Teng, F.-Z., Zhang, H.-F. & Li, S.-G. (2012). Magnesium isotopic systematics of continental basalts from the North China craton: implications for tracing subducted carbonate in the mantle. *Chemical Geology* **328**, 185–194.

Yaxley, G. M., Green, D. H. & Kamenetsky, V. (1998). Carbonatite metasomatism in the southeastern Australian lithosphere. *Journal of Petrology* **39**, 1917–1930.

Zeng, G., Chen, L.-H., Hofmann, A. W., Jiang, S.-Y. & Xu, X.-S. (2011). Crust recycling in the sources of two parallel volcanic chains in Shandong, North China. *Earth and Planetary Science Letters* **302**, 359–368.

Zeng, G., Chen, L.-H., Xu, X.-S., Jiang, S.-Y. & Hofmann, A. W. (2010). Carbonated mantle sources for Cenozoic intra-plate alkaline basalts in Shandong, North China. *Chemical Geology* **273**, 35–45.

Zhang, G.-L., Chen, L.-H., Jackson, M. G. & Hofmann, A. W. (2017). Evolution of carbonated melt to alkali basalt in the South China Sea. *Nature Geoscience* **10**, 229–235.

Zhang, H., Huang, Q., Zhao, G., Guo, Z. & Chen, Y. J. (2016). Three-dimensional conductivity model of crust and uppermost mantle at the northern Trans North China Orogen:

evidence for a mantle source of Datong volcanoes. *Earth and Planetary Science Letters* **453**, 182–192.

Zhang, H.-F., Sun, M., Zhou, M.-F., Fan, W.-M., Zhou, X-h. & Zhai, M.-G. (2004). Highly heterogeneous Late Mesozoic lithospheric mantle beneath the North China Craton: evidence from Sr–Nd–Pb isotopic systematics of mafic igneous rocks. *Geological Magazine* **141**, 55–62.

Zhao, D., Tian, Y., Lei, J., Liu, L. & Zheng, S. (2009). Seismic image and origin of the Changbai intraplate volcano in East Asia: role of big mantle wedge above the stagnant Pacific slab. *Physics of the Earth and Planetary Interiors* **173**, 197–206.

Zhao, H., Liu, Z., Wang, C.-M. & Li, S.-H. (2015). Luminescence dating of volcanic eruptions in Datong, northern China. *Quaternary Geochronology* **30**, 357–362.

Zheng, J., Griffin, W. L., O'Reilly, S. Y., Yang, J., Li, T., Zhang, M., Zhang, R. Y. & Liou, J. G. (2006). Mineral chemistry of peridotites from Paleozoic, Mesozoic and Cenozoic lithosphere: constraints on mantle evolution beneath eastern China. *Journal of Petrology* **47**, 2233–2256.

Zhi, X., Song, Y., Frey, F. A., Feng, J. & Zhai, M. J. C. G. (1990). Geochemistry of Hannuoba basalts, eastern China: constraints on the origin of continental alkalic and tholeiitic basalt. *Chemical Geology* **88**, 1–33.

Zhong, Y., Chen, L.-H., Wang, X.-J., Zhang, G.-L., Xie, L.-W. & Zeng, G. (2017). Magnesium isotopic variation of oceanic island basalts generated by partial melting and crustal recycling. *Earth and Planetary Science Letters* **463**, 127–135.

Zhou, X. & Armstrong, R. L. (1982). Cenozoic volcanic rocks of eastern China-secular and geographic trends in chemistry and strontium isotopic composition. *Earth and Planetary Science Letters* **58**, 301–329.

Zong, K. & Liu, Y. (2018). Carbonate metasomatism in the lithospheric mantle: Implications for cratonic destruction in North China. *Science China Earth Sciences* **61**, 711–729.

Zou, H., Zindler, A., Xu, X. & Qi, Q. (2000). Major, trace element, and Nd, Sr and Pb isotope studies of Cenozoic basalts in SE China: mantle sources, regional variations, and tectonic significance. *Chemical Geology* **171**, 33–47.